

Diffusion Instruction Tuning

Chen Jin¹ Ryutaro Tanno² Amrutha Saseendran¹ Tom Diethe¹ Philip Teare¹

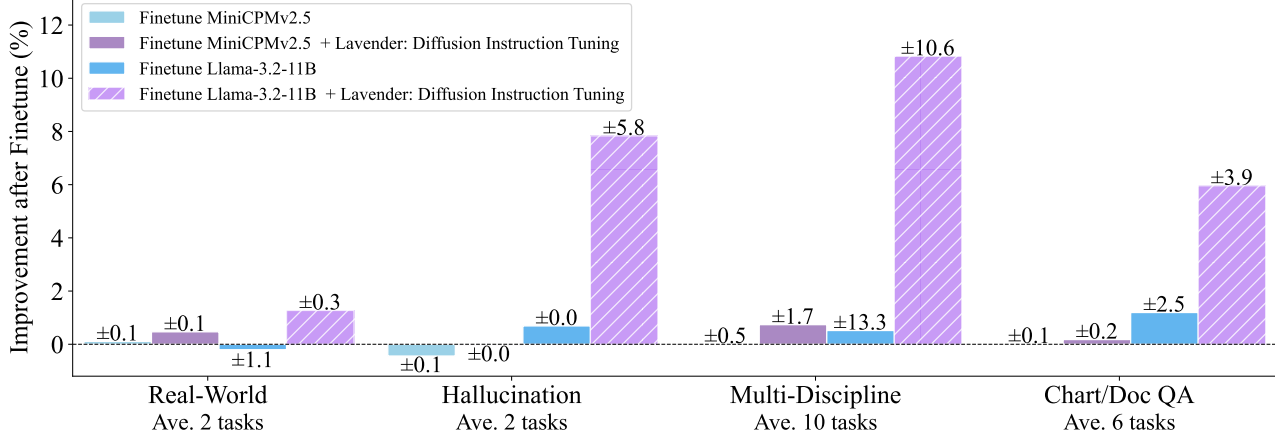


Figure 1. Average Performance on 20 Vision-Language Reasoning Benchmarks (Grouped into 4 Categories).

Abstract

We introduce *Lavender*, a simple supervised fine-tuning (SFT) method that boosts the performance of advanced vision-language models (VLMs) by leveraging state-of-the-art image generation models such as Stable Diffusion. Specifically, *Lavender* aligns the text-vision attention in the VLM transformer with the equivalent used by Stable Diffusion during SFT, instead of adapting separate encoders. This alignment enriches the model’s visual understanding and significantly boosts performance across in- and out-of-distribution tasks. *Lavender* requires just 0.13 million training examples—2.5% of typical large-scale SFT datasets—and fine-tunes on standard hardware (8 GPUs) in a single day. It consistently improves state-of-the-art open-source multimodal LLMs (e.g., Llama-3.2-11B, MiniCPM-Llama3-v2.5), achieving up to 30% gains and a 68% boost on challenging out-of-distribution medical QA tasks. By efficiently transferring the visual expertise of image generators with minimal supervision, *Lavender* offers a scalable solution for more accurate vision-language systems. All code, training data, and models will be shared.

¹Centre for AI, AstraZeneca, Cambridge, UK ²Google DeepMind, UK. Correspondence to: <chen.jin@astrazeneca.com>.

Copyright 2025 by the author(s).

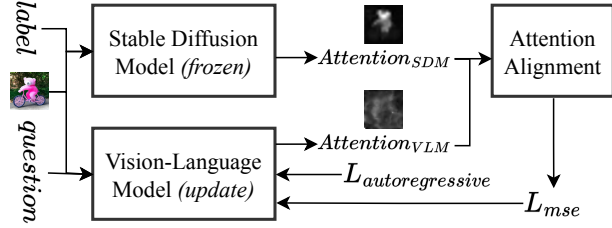


Figure 2. **Lavender: Diffusion Instruction Tuning.** *Lavender* uses the text-vision attention maps of a Stable Diffusion Model, $Attention_{SDM}$, as a guiding objective for the attention of the target vision-language model (VLM), $Attention_{VLM}$. The *Attention Alignment* module employs a 3-Layer ConvNet to transform $Attention_{VLM}$ to match $Attention_{SDM}$ via an MSE loss, acting as a regularisation term during supervised fine-tuning.

1. Introduction

Training frontier foundation models from scratch costs millions of dollars at minimum, requiring hundreds of GPUs and millions to billions of data (DeepSeek-AI et al., 2024). This challenge is even more pronounced in multimodal settings: vision-language models (VLMs) often face data scarcity because collecting paired image-text datasets is expensive (Zhu et al., 2024). A common workaround is to apply supervised fine-tuning (SFT) on a pretrained large language model (LLM), leveraging its abundant text-only pre-training and adjusting bridging layers or additional encoders

with limited image-text pairs (Liu et al., 2024c; Covert et al., 2024; Jiang et al., 2023). However, these methods typically overlook the importance of transformer-level attention alignment within the LLM core—a key component for effectively expanding text-based models into the visual domain.

Precise visual-text alignment is crucial for advanced multi-modal reasoning. While both VLMs and diffusion models (DMs) process text and images, they diverge in their generation objectives. We observe that DMs, such as Stable Diffusion (Rombach et al., 2021), which reconstructs images at the pixel level, appear to learn more precise text-vision attention maps than VLMs that are optimised solely for text token generation (Figure 3).

In this work, we demonstrate that the high-quality cross-attention maps from these DMs indeed offer a useful target for guiding the text-vision attention in VLMs during SFT, thus improving word-to-region alignment and the overall performance. We introduce **Lavender** (Language-and-Vision fine-tuning with Diffusion Aligner), *the first framework to directly align VLM transformer attention layers with those of Stable Diffusion* (Figure 1(c)). Specifically, during SFT, Lavender transfers diffusion-based attention distributions to VLMs, enhancing core visual-textual interactions. To mitigate catastrophic forgetting, we additionally propose several attention aggregation methods and training strategies that preserve existing VLM competencies.

We begin by verifying Lavender on a small OpenFlamingo model: entropy and visual analyses show Lavender aligns VLM attention with DM attention. Leveraging Stable Diffusion to *offline* extract per-word attention on 130k label-image pairs—*no extra training cost*—Lavender yields notable gains over autoregressive finetuning on 20 diverse benchmarks, including up to 70% improvement on OpenFlamingo across seven benchmarks. For Llama 3.2-11B, fine-tuned on in- and out-of-distribution data, performance improves by up to 30% on 19 benchmarks, surpassing comparable small open-source models by 50%. On self-attention-only MiniCPMv2.5, it achieves up to 4% gains.

This advantage extends to severely OOD domains, evidenced by a 68% boost on the WorldMedQA medical benchmark for Llama 3.2-11B. Further analyses reveal that larger fine-tuning sets help Lavender resist overfitting more effectively than autoregressive baselines, and the aligned attention maps yield finer-grained visual understanding. Together with qualitative evidence of improved VLM attention, these results confirm Lavender’s premise: *diffusion-based attention distributions effectively align visual and textual representations*, fostering more robust, data-efficient VLMs.

Ablation studies reveal that the method of attention aggregation and the choice of layers for fine-tuning are critical to performance. Learned aggregation strategies outperform

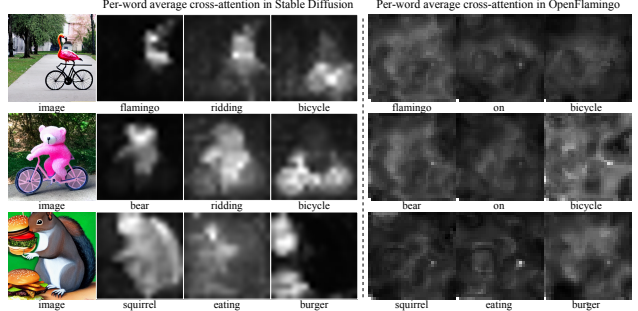


Figure 3. Image generation models (Stable Diffusion on the left) exhibit stronger word-to-region attention alignment than VLMs (Open-Flamingo on the right). Per-word average attention maps suggest that diffusion models may be closer to an ideal distribution correlating image regions with textual tokens.

manual ones and lightweight pretraining of an Aligner Network helps prevent catastrophic forgetting on small datasets. LoRA fine-tuning delivers faster improvements, full finetuning proves more effective for handling complex tasks. Aligning all cross-attention layers proves most effective, highlighting the importance of precise attention alignment.

In summary, we introduce *Lavender*, a novel framework that transfers “visual expertise” from text-to-image diffusion models to vision-language models *without additional annotations*. By aligning attention distributions, Lavender enhances word-to-region grounding, improves fine-tuning efficiency, and boosts model robustness, particularly in out-of-distribution settings. Moreover, our architecture-agnostic attention alignment loss is compatible with RL post-training, offering scalable diffusion-guided feedback instead of costly, subjective human vision feedback. Beyond addressing data scarcity, Lavender demonstrates that pretrained generative models can guide multimodal learning in a scalable and compute-efficient manner. This approach bridges two expert paradigms—language and vision generation—into a more unified, capable system. Our findings suggest broader applications in multimodal AI, offering a modular and privacy-friendly alternative to closed-source models. We open-source our work to encourage further exploration of diffusion-guided alignment, unlocking new possibilities in vision-language reasoning.

2. Related Work

We find that the gap in VLM alignment partly stems from the technological trajectories pursued over the past half-decade. One key VLM milestone was Flamingo (Alayrac et al., 2022), which laid the foundation for modern VLMs. In its design, images and text are processed by separate encoders, unified through a perceiver resampler (Jaegle et al., 2021), and passed through deep transformer layers combining cross-attention and self-attention. Flamingo’s elegant

architecture established a new standard, influencing a range of subsequent models (Li et al., 2022; 2023b; You et al., 2023). The importance of aligning vision-text correlations is evident in the design of Llama 3.2 (Dubey et al., 2024), released two years later, which adopts Flamingo’s strategy of using a dedicated cross-attention module for effective interaction handling. However, training a VLM with a dedicated cross-attention module end-to-end requires substantial data and computational resources. These models are typically pre-trained on millions or even billions of image-text pairs and interleaved image-text datasets (Zhu et al., 2024). Similar challenges apply to broader multimodal models beyond vision and language (Lu et al., 2024).

Unlike VLMs, single-modality large language models (LLMs) have scaled more rapidly (Ouyang et al., 2022; Brown et al., 2020; Chowdhery et al., 2023), often consuming over 100 million examples spanning 1,800 tasks (Longpre et al., 2023). VLMs, however, face a training data gap due to the high cost of acquiring paired image-text datasets. To address this, researchers proposed leveraging scaled LLMs by instruction fine-tuning them on as little as 150k paired visual question answering (VQA) data using an autoregressive loss. This approach, pioneered by Zhu et al. (2023); Dai et al. (2023); Liu et al. (2024c), aligns text and image tokens through fine-tuning connectors such as MLPs, encoders, or decoders connecting to the LLM, providing an efficient pathway to integrate vision with language models for diverse tasks (Wang et al., 2024a; Li et al., 2024; Koh et al., 2024; Chen et al., 2025a; Wang et al., 2024b; Chen et al., 2023; Huang et al., 2024; Liu et al., 2024d; Gao et al., 2023; Cha et al., 2024).

However, the community soon recognised that the vision capabilities integrated through these small adapter layers outside the LLM (in LLaVA-like approaches) remain insufficient (Tong et al., 2024c). To address this gap, Covert et al. (2024); Karamcheti et al. (2024) refined vision encoders to align more closely with pretrained vision models. Jiang et al. (2023); Kar et al. (2025) proposed merging multiple visual encoders with projection layers before feeding them into the LLM. Separately, Tong et al. (2024a); Shi et al. (2024); Zong et al. (2024) explored merging a larger number of diverse vision expert models with fine-tuned projection layers, integrating the combined vision features either before the LLM or within the LLM transformer layers, respectively.

Diffusion Models (DMs), as vision experts, have gained recent attention. Wang et al. (2024c) use DM’s image generation loss to enhance the visual encoder. Other approaches merge VLMs with DM’s image generation, either by fine-tuning DMs with VLM outputs (Tong et al., 2024b; Hernandez et al., 2024), sharing a central transformer (Shi et al., 2025; Chen et al., 2025b), or integrating DMs with LLM transformers (Zhou et al., 2024).

Despite attempts to integrate DMs and VLMs with minimal modifications to their internal architectures, *one overlooked aspect in prior work is the role of self- and cross-attention layers within DM and LLM Transformers*. These layers govern the interplay between multi-modal tokens, yet have not been closely examined. Although DMs and the LLM component in VLMs share the same foundational Transformer architecture (Vaswani, 2017; Dosovitskiy, 2020), they exhibit markedly different text-to-region alignment due to their distinct optimization objectives. Notably, DMs demonstrate stronger alignment than VLMs, as shown in Figure 3.

3. Diffusion Instruction Tuning

We aim to enhance a pretrained Vision-Language Model (VLM) by leveraging attention distributions from a pretrained Diffusion Model (DM). We assume there is an *ideal* attention distribution that maximises VLM performance and that the DM’s attention is closer to this ideal distribution.

3.1. Models and Notation

Vision-Language Model (VLM). Let θ be the VLM parameters, pretrained for tasks such as image captioning or question-answering. It models:

$$p(y_l|x, y_q; \theta). \quad (1)$$

Diffusion Model (DM). Let θ_D be the DM parameters, which remain fixed during our procedure. It models:

$$p(x|y; \theta_D). \quad (2)$$

Attention Distributions. We write:

$$p_{\text{VLM}}(a|x, y; \theta), \quad p_{\text{DM}}(a|x, y; \theta_D), \quad (3)$$

We hypothesise that $p_{\text{DM}}(a|x, y; \theta_D)$ is closer to the optimal posterior attention distribution $p^*(a|x, y)$ than $p_{\text{VLM}}(a|x, y; \theta)$, and the two can be aligned by projecting p_{VLM} into a comparable space using small learnable layers.

3.2. Assumptions

Ideal Attention Hypothesis: An attention distribution $p^*(a|x, y)$ minimises the next-token prediction loss of VLM, L_{VLM} ; **DM Attention Proximity:** Empirically, the DM’s attention is more concentrated (lower entropy) and hence closer to p^* than the VLM’s, supported by Figure 3, experiments in Section 7.1 and detailed justifications in Appendix B; **Shared Dataset:** Both models use the same image-text set $\{(x^{(i)}, y^{(i)})\}$; **Fixed DM Parameters:** θ_D is kept fixed; only θ is updated; **Pretrained VLM Parameters:** θ is further fine-tuned with an attention alignment loss.

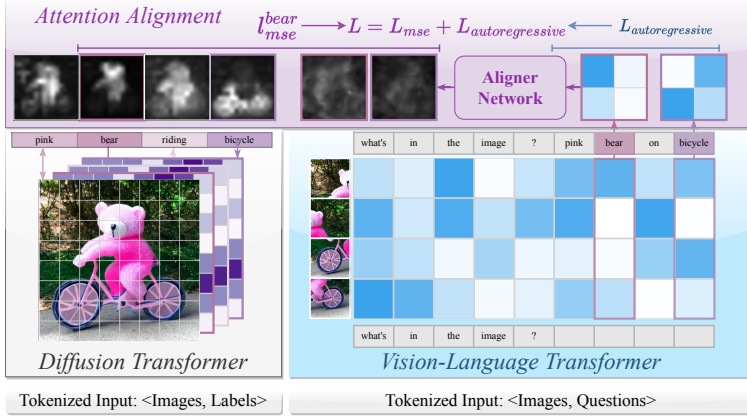


Figure 4. Sketch of Diffusion Instruction Tuning (left) and a short pseudo code (right), whose full version is available in Appendix A.

3.3. Bayesian Derivation

Our objective is to update the VLM parameters θ such that the model not only performs well on its primary task but also aligns its attention mechanism with that of the DM. We formalise this objective within a Bayesian framework.

Posterior Distribution: We aim to find the posterior distribution of the VLM parameters given the data D and the DM's attention distributions:

$$p(\theta|D, A_{DM}) \propto p(D|\theta) p(A_{DM}|\theta) p(\theta), \quad (4)$$

where $A_{DM} = \{p_{DM}(a|x^{(i)}, y^{(i)}; \theta_D)\}$ is the collection of attention outputs derived from the DM's conditional distribution, and $p(\theta)$ is the prior over the VLM parameters.

Likelihood of the Data: The likelihood of the data given θ is:

$$p(D|\theta) = \prod_i p(y_l^{(i)}|x^{(i)}, y_q^{(i)}; \theta). \quad (5)$$

The negative log-likelihood corresponds to the standard loss function $L_{VLM}(\theta)$ used to fine-tune the VLM:

$$L_{VLM}(\theta) = - \sum_i \log p(y_l^{(i)}|x^{(i)}, y_q^{(i)}; \theta). \quad (6)$$

Likelihood of the DM's Attention: We model the likelihood of observing the DM's attention given the VLM's parameters, denoted as $p(A_{DM}|\theta)$. To simplify the notation and make the equations more concise, we introduce:

$$\delta^{(i)}(\theta) = p_{VLM}(a|x^{(i)}, y^{(i)}; \theta) - p_{DM}(a|x^{(i)}, y^{(i)}; \theta_D). \quad (7)$$

This represents the pointwise difference between the VLM's and DM's attention distributions for the i -th data point, serving as a measure of divergence at each attention location a . Assuming that these differences are Gaussian-distributed with equal variance, the likelihood can be expressed as:

$$p(A_{DM}|\theta) \propto \exp\left(-\frac{\lambda}{2} \sum_i \|\delta^{(i)}(\theta)\|^2\right). \quad (8)$$

Algorithm 1 Diffusion Instruction Tuning

```

Require:  $D = \{(x^{(i)}, y^{(i)})\}, \theta_D, \theta$ , scale  $\lambda$ 
Ensure: Fine-tuned VLM parameters  $\theta$ 
Stage 1: Precompute DM Attention (run once)
for each  $(x^{(i)}, y^{(i)}) \in D$  do
     $A_{DM}^{(i)} \leftarrow p_{DM}(a|x^{(i)}, y^{(i)}; \theta_D)$ 
end for
Stage 2: Fine-Tune VLM
repeat
    Sample batch  $B \subseteq D$ , set  $L_{VLM}(\theta) = 0, L_{att}(\theta) = 0$ 
    for each  $(x^{(i)}, y^{(i)}) \in B$  do
        Compute  $p_{VLM}(a|x^{(i)}, y^{(i)}; \theta)$ 
         $\delta^{(i)}(\theta) \leftarrow \text{Aligner}(p_{VLM}(a)) - A_{DM}^{(i)}$ 
         $L_{VLM}(\theta) += -\log p(y_l^{(i)}|x^{(i)}, y_q^{(i)}; \theta)$ 
         $L_{att}(\theta) += \|\delta^{(i)}(\theta)\|^2$ 
    end for
     $L_{total}(\theta) \leftarrow L_{VLM}(\theta) + \lambda L_{att}(\theta)$ 
    Update  $\theta \leftarrow \theta - \eta \nabla_\theta L_{total}(\theta)$ 
until convergence

```

This corresponds to the attention alignment loss $L_{att}(\theta)$:

$$L_{att}(\theta) = \sum_i \|\delta^{(i)}(\theta)\|^2. \quad (9)$$

By minimizing $L_{att}(\theta)$, i.e., the MSE loss, we encourage the VLM's attention to align with that of the DM, guiding it toward the optimal posterior attention distribution $p^*(a|x, y)$.

For simplicity, we assume a non-informative prior $p(\theta)$. Consequently, the posterior distribution in the previous equation Equation (4) is governed primarily by $p(D|\theta)$ and $p(A_{DM}|\theta)$. If regularisation is needed, a more informative prior can be seamlessly incorporated. Combining the terms, the negative log-posterior (up to a constant) becomes:

$$L_{total}(\theta) = L_{VLM}(\theta) + \lambda L_{att}(\theta). \quad (10)$$

Here, λ balances the importance of aligning the attention distributions with the primary task. We fully justify the inclusion of the attention alignment loss in Appendix C.

3.4. Interpretation and Practical Implementation

By minimizing $L_{total}(\theta)$, we maximize $p(\theta|D, A_{DM})$, aligning the VLM's attention closer to the ideal posterior $p^*(a|x, y)$. This improves the VLM's ability to associate textual tokens with relevant visual regions, enhancing vision-text understanding. To implement this, we extract per-word attention distributions from the pretrained DM and VLM:

$$p_{DM}(a|x^{(i)}, y^{(i)}; \theta_D), \quad p_{VLM}(a|x^{(i)}, y^{(i)}; \theta). \quad (11)$$

Fine-tuning minimizes:

$$L_{total}(\theta) = - \sum_i \log p(y_l^{(i)}|x^{(i)}, y_q^{(i)}; \theta) + \lambda \sum_i \|\delta^{(i)}(\theta)\|^2. \quad (12)$$

This model-agnostic process, outlined in Algorithm Algorithm 1, requires no additional data and works with various VLM architectures.

4. Attention Alignment

We discuss how to compute per-word attention in VLMs and DMs. Although both employ attention to capture vision-text interplay, their attention aggregation differs (Figure 4). Understanding these distinctions is key to effective alignment.

4.1. Attention Aggregation in Diffusion Models

Text-guided diffusion models generate images from textual input by iteratively denoising a random-noise image. During each denoising step, *cross-attention* layers enable the model to focus on relevant textual tokens. Specifically, queries Q are derived from the noisy image x_t , while keys K and values V come from the text embedding v :

$$Q = f_Q(x_t), \quad K = f_K(v), \quad V = f_V(v), \quad (13)$$

where f_Q , f_K , and f_V are pretrained projection matrices of DM. The attention map M is then computed as:

$$M = \text{Softmax}((QK^\top)/\sqrt{d}). \quad (14)$$

Prior work (Hertz et al., 2022) shows that averaging these maps across layers and time steps reveals meaningful correspondences between words and image regions. The resulting per-word attention distributions $p_{\text{DM}}(a|x, y; \theta_D)$ indicate salient image regions for each token, as shown in Figure 3. We leverage these maps as a proxy for the optimal posterior attention distribution $p^*(a|x, y)$, guiding the VLM’s alignment toward more focused vision-text interactions.

4.2. Attention Aggregation in Vision-Language Models

Vision-language models (VLMs) use transformer attention to connect text tokens (T_t) with image patch tokens (T_p) across multiple heads and layers, forming attention weights $w_{(t,p)}^{hl}$. These weights capture semantic and spatial relationships between tokens and patches.

To create per-word saliency maps, we first aggregate attention across all heads and layers, reducing the $(N_{\text{text}} \times N_{\text{patch}} \times H \times L)$ tensor to a $(N_{\text{text}} \times N_{\text{patch}})$ matrix. Next, we reshape this matrix into a $\sqrt{N_{\text{patch}}} \times \sqrt{N_{\text{patch}}}$ grid, which approximately reconstructs the spatial layout of the original image (Appendix E). This process generates interpretable saliency maps, where each row highlights how a text token focuses on image patches. These maps allow us to align VLM attention with that of the Diffusion Model (DM), as shown in Figure 5. To explore the best attention aggregation mechanisms for VLMs, we employ various approaches.

4.2.1. SIMPLE AGGREGATION FUNCTIONS

A straightforward approach is to pool attention weights \mathbf{A} (i.e., $w_{(t,p)}^{hl}$) across heads H and layers L via mean or max. We consider four strategies:

$$\mathcal{A}_{\text{mean/max}}^{(L,H)}(\mathbf{A}) \in \{\text{max-max}, \text{max-mean}, \text{mean-max}, \text{mean-mean}\},$$

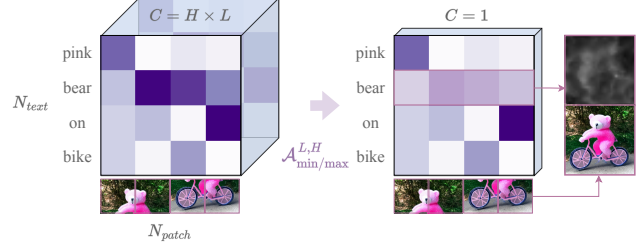


Figure 5. Illustration of attention aggregation in VLMs. Attention weights between text tokens and image patches are aggregated to form per-word saliency maps.

where each denotes a combination of {Max, Mean} over H and L . This yields a single per-word attention map, capturing a coarse measure of word-to-patch alignment.

4.2.2. ATTENTION FLOW

Proposed by Abnar & Zuidema (2020), *attention flow* accumulates attention across multiple layers to track how information propagates through the network. Unlike simple pooling, this method captures deeper dependencies by considering all layers together.

To capture interactions across layers, we recursively update the attention map. Starting with the first layer’s attention $A^{(1)}$, we merge each subsequent layer $A^{(l)}$ using element-wise multiplication or addition:

$$\bar{A} \leftarrow \bar{A} \circ A^{(l)} \quad \text{or} \quad \bar{A} \leftarrow \bar{A} + A^{(l)}.$$

This method, previously applied by Lin et al. (2024) at the *sentence level*, is extended here to finer-grained *word-level attention maps*. By aggregating attention across layers, this approach may highlight semantic relationships that simpler methods overlook. Further details are in Appendix D.

4.2.3. LEARNING THE ATTENTION AGGREGATIONS

Standard approaches aggregate attention using predefined pooling methods, which may lose fine-grained relationships. Instead, we introduce *parallel* cross-attention parameters (W_{Q_d}, W_{K_d}) alongside the pretrained projections (W_Q, W_K). This enables us to *capture richer semantic correlations without overwriting existing weights*.

To retain the benefits of the pretrained attention while incorporating new learned patterns, we compute both the original attention A and a parallel attention A_d during each forward pass. The parallel attention A_d is then used to align with the DM:

$$A = \text{Softmax}((QK^\top)/\sqrt{d_k}), \quad (15)$$

$$A_d = \text{Softmax}((Q_dK_d^\top)/\sqrt{d_k}). \quad (16)$$

Empirically, we find that learning parallel cross-attention

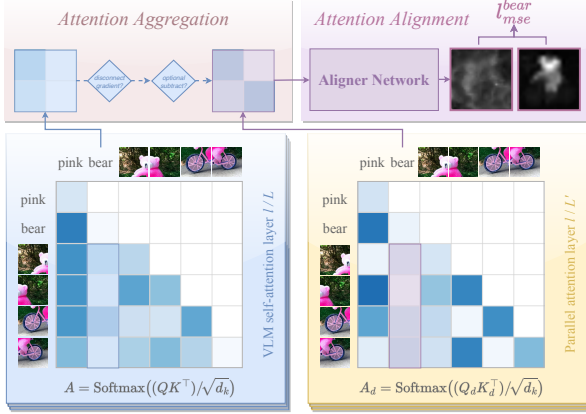


Figure 6. Learning to aggregate with parallel attention. The demonstration is based on a self-attention VLM. The parallel attention constitutes about $1/5^{th}$ of the total VLM layers ($L' \in L$).

in just $1/5^{th}$ of the layers (see Figure 6) is sufficient for effective alignment. This approach balances efficiency with accuracy, preserving the VLM’s core knowledge while benefiting from the DM’s attention distributions.

4.3. Aligner Network

To improve attention alignment between the Vision-Language Model (VLM) and the Diffusion Model (DM), we introduce a lightweight Aligner network. This network refines the parallel (or aggregated) attention A_d into a single-channel map, making it directly comparable to the DM’s attention $p_{\text{DM}}(a|x, y; \theta_D)$. Inspired by Squeeze-and-Excitation networks (Hu et al., 2018), it efficiently transforms attention representations while preserving key semantic information. The Aligner network consists of several small (3-5) layers, using either MLPs or convolutions. First, it expands the representation to capture richer features, applies non-linear transformations, and then compresses it back into a single-channel attention map. Empirically, we found *convolutional layers better capture local spatial cues than MLP*, detailed comparisons are provided in Appendix F.1. During fine-tuning, the Aligner output is compared to the DM’s attention via:

$$L_{\text{att}}(\theta') = \sum_i \| \text{Aligner}(A_d^{(i)}) - p_{\text{DM}}(a|x^{(i)}, y^{(i)}; \theta_D) \|^2, \quad (17)$$

guiding the VLM’s attention toward the DM’s more focused distribution, capturing complex semantic correlations while preserving the original pretrained parameters.

4.4. Lavender Integration

Cross-Attention. For VLMs with dedicated cross-attention layers, each head produces word-to-patch weights $w_{(t,p)}^{hl}$ mapping text tokens T_t to image patches T_p . We

can reshape these weights into spatial grids and aggregate across heads/layers, then apply the Aligner network to yield final per-word saliency maps comparable to DM attention. To ensure consistency, we process the extracted attention weights as follows: 1) Interpolate the attention weights to form a roughly square matrix. 2) Arrange the tiles (if the image is represented as multiple tiles) into a coherent spatial layout (see Figure 23). 3) Resize the maps to a standard resolution (e.g., 32×32) for downstream processing.

Self-Attention Only. When both text and image patches are interleaved in a single sequence, tokens attend to each other in a bidirectional or causal manner. To extract word-to-patch correlations, we must: 1) Identify which subset of tokens corresponds to text and which correspond to image patches. 2) Apply a causal or bidirectional mask to exclude irrelevant attention connections. 3) Reshape and interpolate the extracted attention weights to reconstruct a meaningful spatial representation. This process involves selecting the appropriate text and vision token indices, interpolating attention maps into a square grid, resizing to a fixed resolution (e.g., 32×32), and optionally incorporating the Aligner network output A_d or merged attention maps. This process is demonstrated in Figure 6. By following this procedure, we extract a meaningful per-word attention map aligned with the DM attention, enabling Lavender to improve vision-text alignment even in models that rely exclusively on self-attention.

5. Implementation

We integrate Lavender with three VLMs—cross-attention VLMs (OpenFlamingo, Llama 3.2-11B-Vision Instruct) and self-attention VLMs (MiniCPM-Llama 3-v2.5)—using Stable Diffusion v1.4 (Rombach et al., 2021) to provide per-word attention targets. We introduce a lightweight Aligner network and an attention alignment loss to guide the VLM toward the DM’s more focused distributions.

1) *DM Attention Extraction.* We extract per-word attention maps from Stable Diffusion v1.4 by applying a shortened inversion process (Mokady et al., 2022; Jin et al., 2023) using the paired image-label data. Attention maps are collected at each denoising step and reshaped into a fixed 32×32 resolution. For efficiency, we limit inversion to 5 steps and diffusion to 10 steps, enabling each image to be processed in 20 seconds on a single V100 GPU. 2) *Cross-Attention VLMs.* For OpenFlamingo and Llama 3.2-11B-Vision Instruct, which use cross-attention layers, we integrate Lavender by wrapping the attention layers to extract per-word attention maps. These are then aligned with DM-derived distributions using the Aligner network and attention alignment loss. 3) *Self-Attention VLMs.* For MiniCPM-Llama 3-v2.5, which relies solely on self-attention, we extract

word-to-patch correlations by identifying text and image tokens in the self-attention layers. We reshape and interpolate the extracted attention maps into a structured spatial layout, aligning them with DM attention in the same way as cross-attention models. 4) *Computing Environment*. Experiments are conducted on NVIDIA GPUs (V100, A10G, A100) using PyTorch. For efficient training, we use DeepSpeed with MiniCPM-Llama 3-v2.5 and Fully Sharded Data Parallel (FSDP) for Llama 3.2-11B-Vision Instruct. All models are fine-tuned with Lavender while maintaining their original training procedures and hyperparameters.

6. Training Strategies and Dataset Preparation

Training Strategies. We adopt several strategies to stabilise alignment objectives and preserve a VLM’s pretrained capabilities: 1) *Pretraining the Aligner Network*. Before updating all parameters, we optionally *pretrain only the Aligner network*, freezing the rest of the model to absorb DM-based attention signals without disrupting existing representations. This stabilises early training and prevents immediate overwriting of pretrained features. 2) *Attention Aggregation and Normalisation*. We experiment with different attention aggregation techniques (Section 4) and apply instance or batch normalisation within the Aligner network to control variance, making the final attention distributions more stable and interpretable. 3) *Configurable Aligner Network*. The Aligner is configurable in depth, allowing trade-offs between efficiency and accuracy. We experiment with “light” (single-layer), “sim” (two-layer), and “deep” (four-layer) variants to balance computational complexity and performance. 4) *Parameter-Efficient Fine-Tuning (PEFT)*. We incorporate PEFT (e.g., LoRA) to prevent catastrophic forgetting by restricting updates to a small, controlled parameter subset. This improves stability and preserves pretrained VLM knowledge. 5) *Sampling Strategies*. We define two approaches for selecting predicted words for alignment: a) *Root word match* (allows lemmatized matches, reducing over-strict alignment constraints). b) *Exact word match* (requires exact token match for stricter supervision).

Dataset Preparation. We process images with Stable Diffusion to obtain per-word attention targets across four datasets: 1) *Flickr30k* (Young et al., 2014): 31,783 images, 158,915 captions, focused on everyday human activities. 2) *Laion50k* (Schuhmann et al., 2022): A 50k subset of Laion-5B (5.85B image-text pairs), used for additional method verification. 3) *RLAIF-V 83k* (Yu et al., 2024): A large-scale multimodal dataset provides 83,132 preference pairs covering multiple sources (MSCOCO, ShareGPT-4V, MovieNet, VQA variants). 4) *OCRVQA30k*: A 30k subset of OCR-VQA, containing text-rich images with associated question-answer pairs. All datasets are processed with DMs to extract attention maps and scaled across different VLMs,

with Laion50k used primarily for OpenFlamingo validation.

7. Experiments and Results

We first validate Lavender on a small-scale setup with OpenFlamingo (Section 7.1) before scaling it to MiniCPMv2.5 (Yao et al., 2024) and Llama 3.2-11B-Vision Instruct (Dubey et al., 2024). We evaluate these models on 20 standard VLM benchmarks, comparing them against 23 baseline models (Section 7.2). To further analyse performance, we conduct data overlap analysis (Section 7.3), investigate scaling behaviour and training efficiency (Section 7.4), and examine out-of-distribution generalisation in medical QA benchmarks (Section 7.5). Finally, we present qualitative results, including aligned attention visualisations and VQA examples, using Llama 3.2-11B (Section 7.6).

7.1. Empirical Verification

We begin by validating the key hypothesis that *DM attention distributions are more concentrated and closely approximate an ideal posterior attention for VLMs* (Section 3.2).

1. *DM attention has lower entropy than VLM attention*. We compare attention entropy across Flickr30k, RLAIF-V83k, and OCRVQA30k, using three VLMs (OpenFlamingo, MiniCPM-v2.5, and Llama 3.2-11B). As shown in Figure 7, the DM’s attention entropy is consistently lower, supporting its proximity to the optimal posterior attention $p^*(a|x, y)$.

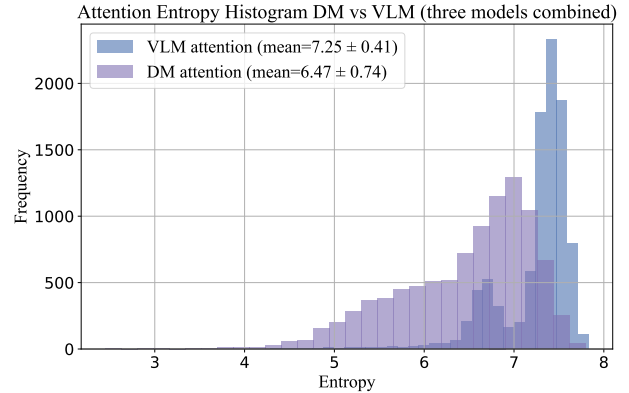


Figure 7. DM attention is more concentrated than VLM attention, aligning closer to the optimal posterior distribution $p^*(a|x, y)$. Measured across OpenFlamingo, MiniCPM-v2.5, and Llama 3.2-11B. Full results in Appendix F.1.

2. *Lavender aligns VLM attention with DM attention*. We fine-tune OpenFlamingo with Lavender on Flickr30k and visualise attention alignment over multiple training steps (Figure 8). The best alignment is achieved using: 1) *Exact word match sampling* instead of root word match. 2) *Convolutional Aligner networks* instead of MLP. 3) *Moderate learning rates* (e.g., $1e-4$ instead of $1e-5$).

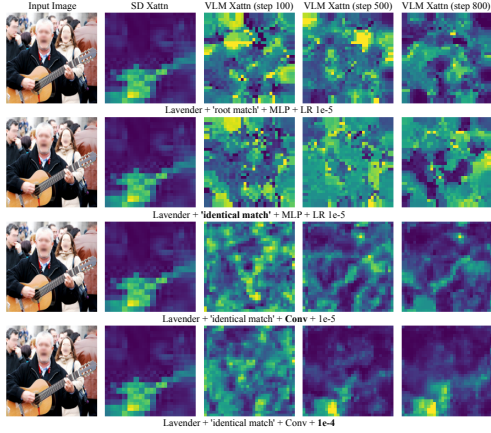


Figure 8. Aligning VLM attention with DM for “guitar.” Each row adds a training technique. More examples in Appendix F.1.

3. Jointly minimising L_{VLM} and L_{att} improves text generation. To test whether Lavender enhances text generation quality, we train OpenFlamingo with Lavender on Flickr30k and Laion50k and evaluate COCO captioning scores. As shown in Figure 9, *MSE loss reduction correlates with higher text generation quality*, confirming that aligning attention improves downstream performance.

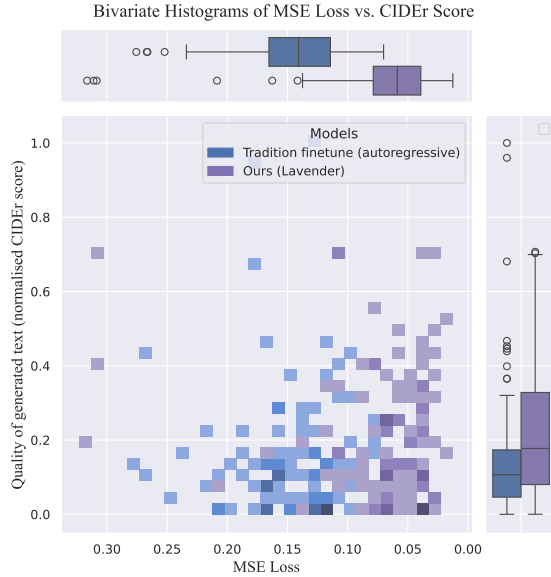


Figure 9. Lower MSE aligns with higher caption quality. Results on COCO, fine-tuning OpenFlamingo with Flickr30k.

4. Lavender boosts zero-shot performance across multiple benchmarks. We compare OpenFlamingo fine-tuned with Lavender against standard autoregressive fine-tuning on seven VLM benchmarks, covering captioning (COCO (Chen et al., 2015) and Flickr30K (Young et al., 2014)), VQA (VQAv2 (Antol et al., 2015), OK-VQA (Marino et al., 2019),

TextVQA (Singh et al., 2019), and VizWiz (Gurari et al., 2018)), and ranking (HatefulMemes (Kiela et al., 2020)). Results in Figure 10 show *up to 72% improvement in zero-shot accuracy*, demonstrating Lavender’s effectiveness in vision-text alignment.

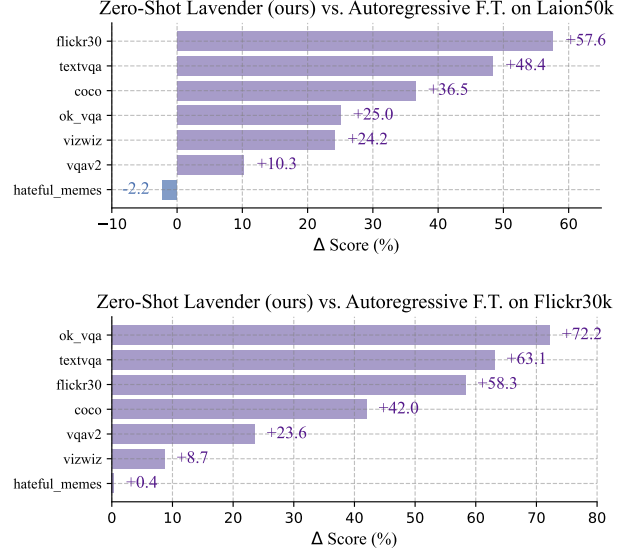


Figure 10. Lavender surpasses autoregressive fine-tuning by up to 72% across seven zero-shot benchmarks. Models are trained on either the Laion50k or Flickr30k dataset.

7.2. Scaled Results with Lavender

After validating Lavender on small-scale fine-tuning with OpenFlamingo, we scale experiments using the Llama 3-based MiniCPMv2.5 and Llama 3.2-11B-Vision-Instruct implementations. Fine-tuning is conducted on a mixture of RV83k, Flk30k, and OV30k datasets, using both autoregressive and Lavender methods, with LoRA or full fine-tuning strategies. We evaluate these models on *20 multimodal benchmarks*, comparing against 23 baseline VLMs.

Evaluation on Multimodal Benchmarks Lavender is evaluated across 20 VLM benchmarks, grouped into four categories: 1) *Chart, Diagram, and Document Understanding*: AI2D (Kembhavi et al., 2016), ChartQA (Masry et al., 2022), OCRBench (Liu et al., 2023c), OCRVQA (Mishra et al., 2019), TextVQA (Singh et al., 2019), DocVQA (Mathew et al., 2021), and InfoVQA (Mathew et al., 2022). 2) *Perception and Multi-Discipline Reasoning*: MME (Fu et al., 2023), MMBench (four subsets) (Liu et al., 2023b), ScienceQA (Saikh et al., 2022), MMStar (Chen et al., 2024a), and MMMU (Yue et al., 2024). 3) *Real-World Visual Understanding*: RealworldQA (x.ai), SEED (Li et al., 2023a). 4) *Hallucination Detection*: HallucinationBench (Liu et al., 2023a) and POPE (Li et al., 2023c). All benchmarks are evaluated using their default metrics.

Baseline Models. In addition to MiniCPMV2.5 (Yao et al., 2024) and Llama 3.2-11B (Dubey et al., 2024) and their fine-tuned variants as baselines, we include the following groups of VLMs and their performance on the above benchmarks as reference: 1) *Small Budget-Constrained Models*. This group consists of open-source VLMs with sizes smaller than 10B, using backbones from Vicuna-7B (Zheng et al., 2023), Qwen-7B (Bai et al., 2023), or Llama3-8B (Dubey et al., 2024). Models include: LLaVA-1.5-7B (Liu et al., 2024a), LLaVA-Next-7B (Liu et al., 2024b), Mini-Gemini-7B (Team, 2024), Eagle-X5-8B (Shi et al., 2024), and Cambrian-1-8B (Tong et al., 2024a). 2) *Small Data-Heavy SOTA Models*. This group includes open-source VLMs with sizes smaller than 20B, typically fine-tuned on datasets containing more than 5M samples. Models in this category are: LLaVA-OneVision-7B (Li et al., 2024), InternVL2-8B (Chen et al., 2024b), Qwen2-VL-7B (Wang et al., 2024a), Molmo-7B (Deitke et al., 2024), and Pixtral-12B (Agrawal et al., 2024). 3) *Large SOTA Models*. This group comprises large VLMs with sizes greater than 20B, including both open- and closed-source models, typically fine-tuned on extensive datasets (minimum 5M samples). Models include: Cambrian-1-34B (Tong et al., 2024a), LLaVA-OneVision-72B (Li et al., 2024), Qwen2-VL-72B (Wang et al., 2024a), Molmo-72B (Deitke et al., 2024), Claude-3 Haiku (Anthropic, 2024), Claude-3.5 Sonnet (Anthropic, 2024), GPT-4V (OpenAI, 2023), GPT-4o (OpenAI, 2024), Gemini 1.5 Pro (Team, 2024), and Llama-3.2-90B (Li et al., 2024).

Main Results with MiniCPM-V-2.5. Figure 15 (a) presents results for MiniCPM-V-2.5, a self-attention-only model based on Llama3. Compared to autoregressive fine-tuning, Lavender improves performance on 16 out of 20 tasks by up to 4%, while limiting drops to a maximum of -1%. The modest overall gains are expected due to dataset reuse (RV83k) and the inherent difficulty of applying text-vision alignment to a purely self-attention model. Nonetheless, *Lavender consistently enhances performance even on saturated datasets, demonstrating its capacity to refine modern VLMs without additional data.*

Main Results with Llama 3.2-11B-Vision-Instruct. Figure 15 (b) presents results for Llama 3.2-11B-Vision-Instruct, a cross-attention-equipped model fine-tuned with both LoRA and full fine-tuning. Lavender outperforms autoregressive fine-tuning by up to 30% on 19 out of 20 benchmarks with LoRA and up to 25% on 17 out of 20 benchmarks with full fine-tuning. These results highlight Lavender’s stronger improvements on cross-attention-based VLMs (Llama 3.2 and OpenFlamingo) compared to the self-attention-only MiniCPM-V-2.5, reinforcing that *the principle of text-vision alignment underlying Lavender is fundamentally rooted in cross-attention mechanisms*

Benchmarking Lavender Against External Baselines. Lavender enhances VLM performance beyond standard next-token prediction fine-tuning. To contextualise its improvements, we compare it against a broad set of baseline models across 16 benchmarks. Figure 12 presents key insights, while Table 1 provides detailed comparisons across three baseline categories.

For *Small Budget-Constrained Models*, Lavender outperforms most benchmarks, achieving up to 50% gains, with minor deficits (within 4%) on benchmarks like SEED-IMG. Among *Small Data-Heavy SOTA Models*, although these models are trained on significantly larger datasets (38x–384x more data), it highlights improvements over the autoregressive baseline, with observed gaps largely attributed to dataset composition (Section 7.3). Finally, for *Large SOTA Models*, Lavender demonstrates competitive performance with select closed-source models an order of magnitude larger (e.g., Claude-3.5 Sonnet, GPT-4o, Gemini 1.5 Pro) on key benchmarks such as TextVQA, POPE, RealWorld, and DocVQA, as shown in Figure 11.

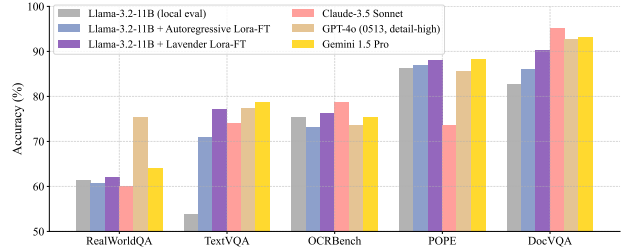


Figure 11. Lavender demonstrates comparable performance to certain High-Resource State-of-the-Art Models.

7.3. Data Overlapping Analysis

Qualitative Analysis. A key question arising from the above benchmark results is how to interpret the observed absolute numbers. In this section, we analyse the overlapping between the disclosed fine-tuning datasets and the benchmark datasets. We perform an ad-hoc qualitative analysis based on the composition of fine-tuning and benchmark datasets to reflect their potential overlapping, as detailed in Figure 13. The qualitative results suggest that the fine-tuning datasets of some state-of-the-art models may exhibit stronger overlapping with the benchmark datasets compared to models fine-tuned on smaller datasets. Lavender’s fine-tuning dataset shows an overlap score on the lower end, similar to LLaVA-1.5 (Liu et al., 2024a), which demonstrates its strong generalizability. This simple approach does not exclude the possibility of data overlap during the pretraining stage, but our focus is on fine-tuning, where overfitting is more likely to occur with small fine-tuning datasets.

Diffusion Instruction Tuning

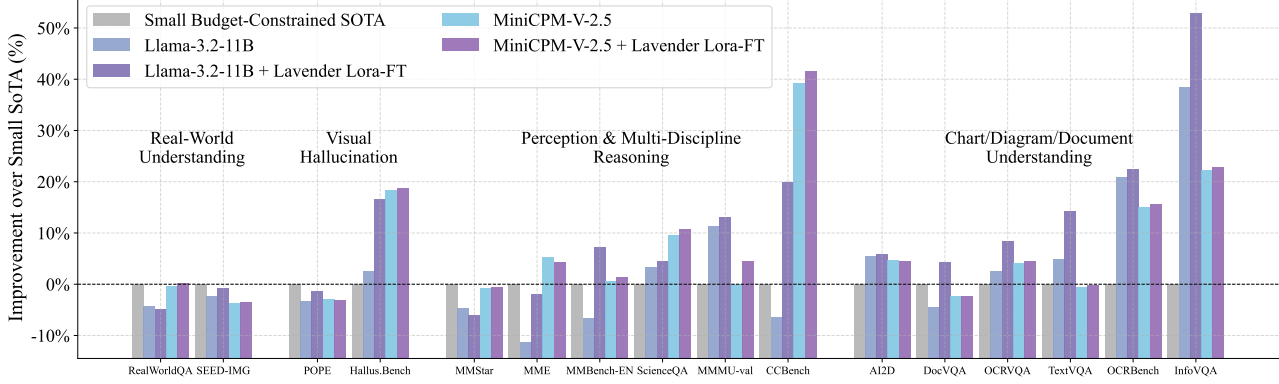


Figure 12. Lavender improves MiniCPM-V-2.5 and Llama-3.2-11B, surpassing Small Budget-Constrained SOTA by up to 50%. This plot highlights the key zero-shot accuracy results across 16 VLM benchmarks from Table 1, focusing on Small Budget-Constrained Models. Lavender shows its greatest improvements in *Chart, Diagram, and Document Understanding*, relying on precise text-visual alignment in OCR tasks. Moderate gains are observed in *Perception and Multi-Discipline Reasoning* and *Hallucination*, while the weakest improvements occur in *Real-World Visual Understanding*, which requires broader knowledge.

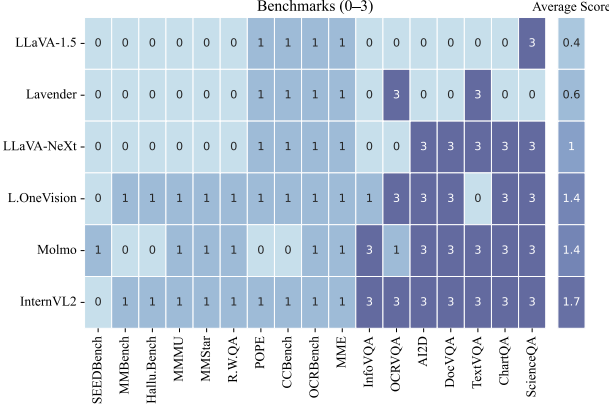


Figure 13. Lavender exhibits minimal data overlap during fine-tuning, supporting its generalisability. Overlap scores are assigned as follows: 3 for explicitly shared benchmark datasets, 1 for datasets with shared sources (e.g., COCO) or web-crawled images, and 0 for no overlap. These estimates are based on publicly available dataset information and highlight Lavender’s robustness on out-of-distribution benchmarks.

7.4. Scaling Behaviour

Lavender is a model-agnostic approach tested on small fine-tuning datasets due to computational constraints. To assess scalability, we fine-tune Llama-3.2-11B on combinations of RV83k, Flk30k, and OV30k using autoregressive and Lavender methods with LoRA or full fine-tuning. Figure 27 presents average performance across eight benchmarks, with detailed results in Figure 28. The findings indicate that Lavender scales better with increased data, effectively reducing overfitting—a common issue with autoregressive fine-tuning on small datasets.

7.5. Severely Out-of-Distribution Medical Benchmark

We evaluate model generalisation on the extreme OOD WorldMedQA-V (Duan et al., 2024), a multilingual, multimodal medical VQA dataset. It includes 568 multiple-choice questions in four low-resource languages, paired with medical images. The dataset’s focus on medical exams and rare languages makes it ideal for testing generalisation beyond typical fine-tuning domains. Figure 16 shows that Lavender improves Llama-3.2-11B’s performance by 68%, surpassing six open-source models (6B–34B) and narrowing the gap with large closed-source models from 43% to 10%.

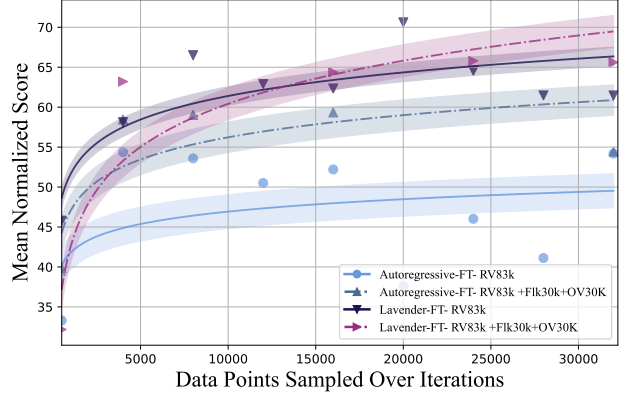
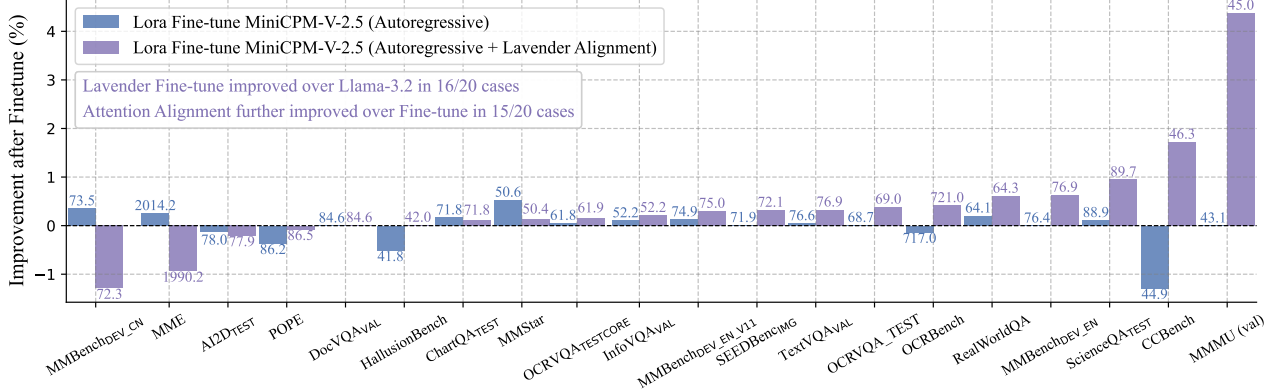
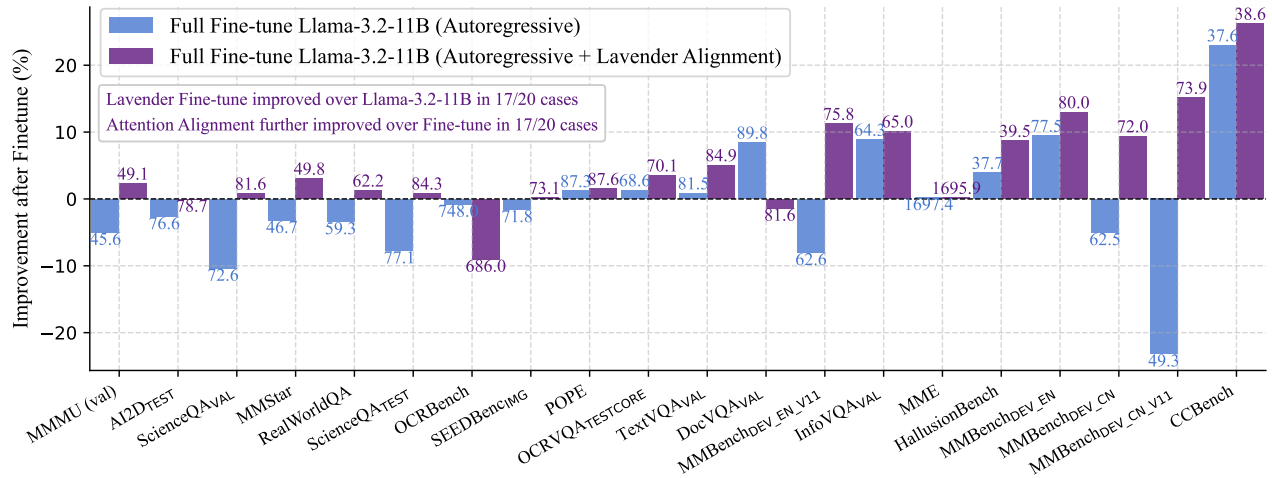
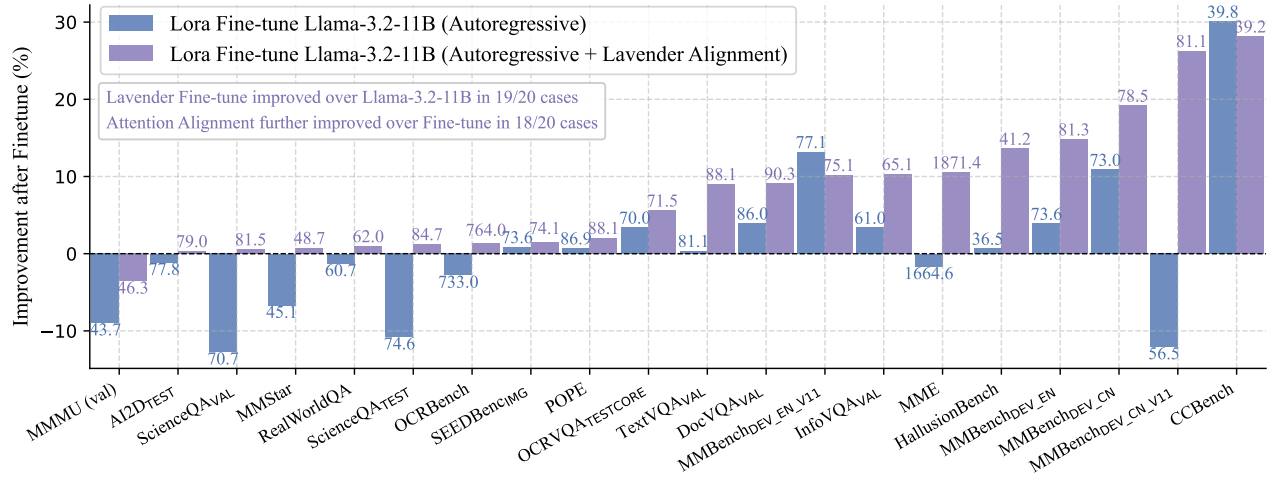


Figure 14. Lavender scales better and mitigates overfitting compared to autoregressive fine-tuning, with larger datasets reducing variability. This plot shows the mean normalised performance across eight benchmarks for two dataset configurations after fine-tuning Llama 3.2-11B. Markers indicate observed performance with trendlines, and shaded regions show variability as 1 standard deviation around the mean. Full results with four dataset configurations are in Appendix Figure 27 and Figure 28.

Diffusion Instruction Tuning



(a) Lavender enhances MiniCPM-Llama3-V-2.5 despite further fine-tuning on its pre-trained dataset.



(b) Lavender mitigates catastrophic forgetting for Llama-3.2-11B fine-tuned on a new dataset.

Figure 15. Relative Improvement Over Baseline on 20 Benchmarks. (a) Results for MiniCPM-Llama3-V-2.5 fine-tuned on its original RV83k dataset. Lavender improves performance on 16/20 benchmarks with gains up to 4%, while limiting performance drops to -1%, primarily on an out-of-distribution Chinese benchmark. (b) Results for Llama-3.2-11B-Vision-Instruct fine-tuned on a mixture of RV83k, Flk30k, and OV30k using LoRA and full fine-tuning strategies. Lavender outperforms autoregressive fine-tuning on 18/20 (LoRA) and 17/20 (Full-FT) benchmarks, achieving up to 30% and 25% improvement, respectively, while mitigating catastrophic forgetting. Across both models, Lavender demonstrates consistent benefits over autoregressive fine-tuning, particularly in reducing catastrophic forgetting.

Diffusion Instruction Tuning

Model	Base	FT Data	Diffusion Instruction Tuning Performance																	
			A12D	CCBench	DocVQA	InfoVQA	MMBench ^{EN}	MME	MMU-val	MMStar	OCRBench	OCRVQA-TQ	POPE	R.W.QA	SEED-IMG	ScienceQA	TextVQA	Hallu.Bench		
Small Budget-Constrained Models (self-attention only)																				
LLaVA-1.5-7B	Vicuna-7B	0.15M	55.5	17.8	28.1	25.8	66.5	1510.0	35.7	33.1	318.0	60.6	86.1	54.8	58.6	69.2	58.2	27.6		
LLaVA-NeXt-7B	Vicuna-7B	0.76M	67.0	24.3	74.4	37.1	67.4	1519.0	37.6	37.6	532.0	63.8	87.5	57.8	70.2	70.3	64.9	27.6		
Mini-Gemini-7B	Qwen-7B	1.5M	-	-	-	-	65.8	1523.0	36.8	-	477.0	-	-	-	-	71.1	65.2	-		
Cambrian-1-7B	Vicuna-7B	10M	74.6	23.7	47.9	40.8	74.6	1802.9	41.8	50.7	614.0	66.0	86.4	60.0	73.3	81.0	77.1	30.6		
Eagle-X5-7B	Vicuna-7B	0.93M	73.6	28.4	86.6	-	68.8	1866.0	37.6	41.7	551	64.3	89.3	63.8	73.6	71.2	71.9	35.4		
LLaVA-1.5-8B	Lama3-8B	0.15M	69.9	27.8	32.4	27.5	-	1825.5	39.2	46.1	420.0	61.0	87.3	56.7	70.1	72.2	-	28.7		
LLaVA-Next-8B	Lama3-8B	0.76M	72.8	32.7	78.5	38.2	74.8	1908	43.1	43.9	531.0	60.7	87.1	58.4	72.5	73.1	65.3	33.1		
Cambrian-1-8B	Lama3-8B	10M	73.0	-	77.8	42.6	75.9	1547.0	42.7	50.7	624.0	66.0	73.0	64.2	74.7	73.1	71.7	30.6		
MiniCPM-V-2.5	Lama3-8B	0.08M	78.1	45.5	84.6	52.1	76.4	2009.1	43.1	50.3	718.0	68.7	86.6	63.9	71.9	88.8	76.6	41.9		
+Lora FT	Lama3-8B	0.08M	77.9	44.9	84.6	52.2	76.4	2014.2	43.1	50.6	717.0	68.8	86.2	64.1	71.9	88.9	76.6	41.8		
+Lavender FT	Lama3-8B	0.08M	77.9	46.3	84.6	52.3	76.9	1990.2	45.0	50.4	721.0	69.0	86.5	64.3	72.1	89.7	76.9	42.0		
Llama-3.2-11B (cross-attention)																				
Llama-3.2-11B	LM32-11B	N.A.	78.7	30.6	82.8	59.0	70.8	1692.9	48.0	48.3	754.0	67.7	86.3	61.4	72.9	83.6	80.8	36.3		
+ AutoR. Lora-FT	LM32-11B	0.13M	77.8	39.8	86.0	61.0	73.6	1664.6	43.7	45.1	733.0	70.0	86.9	60.7	73.6	74.6	81.1	36.6		
+ Lavender Lora-FT	LM32-11B	0.13M	79.0	39.2	90.3	65.1	81.3	1871.5	46.3	48.7	764.0	71.5	88.1	62.1	74.1	84.7	88.1	41.3		
+ AutoR. Full-FT	LM32-11B	0.13M	76.7	37.6	89.8	64.3	77.5	1697.4	45.6	46.8	748.0	68.6	87.3	59.4	71.8	77.1	81.5	37.7		
+ Lavender Full-FT	LM32-11B	0.13M	78.7	38.6	81.6	65.0	80.0	1695.9	49.1	49.8	686.0	70.1	87.6	62.2	73.1	84.3	84.9	39.5		
Small Data-Heavy SOTA Models (<20 B) with Massive FT Data (≥5M)																				
L.OneVision-7B	Qwen-7B	5.2M	82.4	54.9	87.5*	68.8*	83.2	1993.6	47.9	61.9	622.0	64.7	88.4	69.9	76.7	95.4	78.3*	31.6		
InternVL2-8B	InternVL2-8B	5M	83.6	77.1	91.6*	74.8*	81.7*	2215.1	51.2	61.5	794.0	42.6	84.2	64.2	75.4	97.1	77.4*	45.0		
Qwen2-VL-7B	Qwen2-7B	~50M	83.0	65.7	94.5*	76.5*	83.0*	2276.3	53.7	60.7	843.0	67.5	88.4	68.5	76.0	85.5	84.3*	50.4		
Molmo-7B-O	Qwen2-7B	~35M	90.7	20.6	90.8	70.0	69.1	1714.7	39.3	50.1	666.0	15.1	86.7	67.5	72.7	88.8	80.4	42.5		
Pixtral-12B	Nemo-12B	N.A.	79.0	37.6	90.7	50.8	77.9	1921.7	52.5	54.5	685.0	64.7	84.2	65.4	71.5	87.2	75.7	47.0		
Large State-of-the-Art Models (>20 B) with Massive FT Data (≥5M)																				
Cambrian-1-34B	Yi-34B	10M	79.7	49.2	75.5	46.0	81.4	1689.0	49.7	54.2	600.0	68.2	79.7	67.8	75.3	76.8	76.7	41.6		
L.OneVision-72B	Qwen2-72B	5.2M	85.6	63.9	91.3	74.9	85.8	2257.4	56.8	65.8	741.0	-	86.6	71.9	77.5	90.2	80.5	47.9		
Qwen2-VL-72B	Qwen2-72B	~50M	88.1	69.8	96.5	84.5	86.5	2482.7	64.5	68.3	877.0	73.7	87.2	77.8	77.9	91.2	85.5	58.1		
Molmo-72B	Qwen2-72B	~35M	96.3	-	93.5	81.9	79.4	1992.0	54.1	63.3	701.0	-	-	75.2	-	-	83.1	46.6		
Claude-3 Haiku	N.A.	N.A.	86.7	24.5	88.8	56.1	60.7	1920.0	50.2	38.1	658.0	-	74.4	45.5	63.3	-	67.3	39.2		
Claude-3.5 Sonnet	N.A.	N.A.	94.7	54.1	95.2	74.3	79.7	1920.0	68.3	62.2	788.0	-	73.6	60.1	72.2	88.9	74.1	49.9		
GPT-4V (0409)	N.A.	N.A.	89.4	57.3	87.2	75.1	81.0	2070.2	63.1	56.0	656.0	-	81.8	61.4	73.0	84.8	78.0	43.9		
GPT-4o (0513)	N.A.	N.A.	94.2	71.2	92.8	79.2	83.4	2310.3	69.1	63.9	736.0	-	85.6	75.4	77.1	90.7	77.4	55.0		
Gemini 1.5 Pro	N.A.	N.A.	94.4	28.4	93.1	81.0	73.9	2110.6	62.2	59.1	754.0	12.3	88.2	64.1	76.0	85.7	78.7	55.9		
Llama-3.2-90B	Llama-3.1-70B	N.A.	92.3*	54.1	85.7	-	80.4	1741.0	60.3	55.3	783.0	-	86.3	68.2	76.8	87.1	-	44.1		

Table 1. Zero-shot accuracy of various fine-tuned models across 16 VLM benchmarks. Results are grouped into four sections based on base model size and the scale of the fine-tuning dataset. The top score for each benchmark within each group is highlighted in bold. Scores for MiniCPM-V-2.5, Llama-3.2-11B, and their autoregressive (AutoR.) and Lavender fine-tuned variants are locally evaluated using OpenCompass Vlmevalkit (Duan et al., 2024) with ‘gpt-4o’ as the evaluator. All other scores are sourced from the OpenCompass Multi-Modal Leaderboard, evaluated with the same Vlmevalkit. When leaderboard results are unavailable, the models’ published numbers are cited, marked with a * notation if provided. Our observations are categorized as follows: 1) *Small Budget-Constrained Models*. This group is most comparable to Lavender in terms of parameter size and fine-tuning data scale. Both Lavender versions outperform the majority of benchmarks with significant margins over the second-best-performing external models, achieving improvements of up to 40% on CCBench. On a few benchmarks (e.g., MMStar, POPE, and SEED-IMG), Lavender is surpassed by baseline models, though the difference is within 4% for SEED-IMG. Lavender-Llama-3.2 occasionally underperforms on MME due to privacy protection constraints (see Table 3). 2) *Small Data-Heavy SOTA Models*. The primary argument for Lavender in this work is its ability to achieve improvements over the autoregressive fine-tuning baseline. Lavender implementations on MiniCPMv.2.5 and Llama-3.2-11B are not designed to beat state-of-the-art results due to the limited fine-tuning data scale (0.13M), which is significantly smaller than the 5M to 50M datasets used for this group, approximately 38x to 384x larger than that used for Lavender. We simplify the comparison by excluding pretraining dataset sizes for base models. In this group, Qwen2-VL-7B and LLaVA-OneVision-7B are the top performers, surpassing Lavender on most benchmarks. However, we note that the performance gap is likely influenced by the composition of fine-tuning datasets, as discussed in Section 7.3. 3) *Large SOTA Models*. Finally, we include results from the latest state-of-the-art models, which are at least 20B in size (or unreleased models typically exceeding 100B) and fine-tuned on datasets of at least 5M samples. Despite Qwen2-VL-72B outperforming all other models on 18/20 benchmarks, Lavender pushes the boundaries of Llama-3.2-11B, achieving performance comparable to certain closed-source models that are at least an order of magnitude larger (e.g., Claude-3.5 Sonnet, GPT-4o, and Gemini 1.5 Pro) on benchmarks such as TextVQA, POPE, RealWorld, and DocVQA.

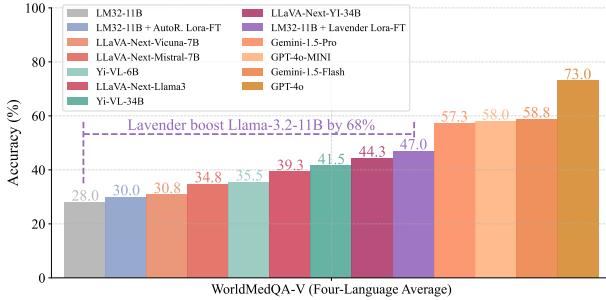


Figure 16. Lavender boosts Llama-3.2-11B’s performance on the OOD WorldMedQA benchmark by 68%. Results are based on fine-tuning Llama-3.2-11B-Vision-Instruct on RV83k, Flk30k, and OV30k using autoregressive or Lavender methods with LoRA. Accuracy reflects average performance across four low-resource medical VQA subsets, evaluated via Vlmevalkit (Duan et al., 2024). Example results in Appendix Table 2.

7.6. Qualitative Results with Llama 3.2-11B.

Visual Results of Aligned Attention Maps. A key argument of Lavender is its ability to align the attention maps of VLMs to those of DMs. Figure 17 provides examples of the cross-attention maps from Llama 3.2-11B after full fine-tuning with Lavender. The results indicate that the aligned VLM attention maps generally correlate with the semantic regions of corresponding words in a manner similar to the Diffusion Model. Interestingly, the VLM attention maps after alignment are more concentrated than those of the Diffusion Model. This difference is likely driven by their distinct optimization goals: sense understanding for optimal text generation in VLMs versus pixel-level precision for image generation in DMs.



Figure 17. The per-word VLM attention maps are aligned to the Stable Diffusion (SD) after tuning with Lavender. Results are from Lavender-Llama 3.2-11B implementation. More results are available in Appendix Figure 30.

Visual Results on VQA Benchmarks. Figure 18 showcases nine VQA examples from multiple evaluated benchmarks, including document, chart, and graphic understanding, real-world OCR, geometry math, visual hallucination,

and medical VQA. The comparison highlights the performance of Llama-3.2-11B-Vision-Instruct (Dubey et al., 2024) against its Lavender fine-tuned version. Overall, Lavender demonstrates significantly improved visual understanding compared to the original Llama-3.2 across various VQA tasks, including DocVQA, TextVQA, ChartQA, and WorldMedQA-V. These improvements stem from Lavender’s ability to accurately localise and interpret visual elements, leading to better performance on questions requiring detailed visual reasoning. A detailed analysis of these examples is provided in the image caption of Figure 18.

8. Ablation and Analysis

We conducted extensive ablation studies to assess the key components of Lavender and their impact on performance. Unless otherwise specified, *all experiments in this section use ‘exact match’ in VQA assessments without an LLM judge for cost efficiency*.

Key findings include: 1) *Attention Aggregation*: Learned aggregation consistently outperforms manual methods like attention flow due to its adaptability and scalability (Figure 19, Figure 20). 2) *Pretraining the Aligner*: Pretraining significantly mitigates catastrophic forgetting, with longer pretraining benefiting more complex benchmarks (Figure 21). 3) *Fine-tuning Strategy*: LoRA achieves better short-term results, while full fine-tuning excels on complex tasks, suggesting complementary benefits (Figure 15) (b). 4) *Layer Alignment*: Aligning all eight cross-attention layers in Llama-3.2-11B proves most effective, outperforming partial alignments (Figure 22).

8.1. Attention Aggregation Functions

We evaluate different attention aggregation strategies in VLMs, including simple averaging (‘layer-mean’), maximisation (‘layer-max’ and ‘max-max’), attention flow combined with multiplicative and additive aggregations (‘flow-multi’ and ‘flow-sum’), and learned aggregation (‘learn’), as detailed in Section 4.

Comparison Across Eight Benchmarks. We fully fine-tune Lavender-Llama 3.2-11B on Flickr-1k for 20 epochs and evaluate all methods on eight benchmarks using ‘exact match’ in VQA assessments. This differs from the main results (Table 1) and leads to an expected 10%–20% performance drop. Figure 19 shows that ‘flow-multi’ performs the weakest, likely due to excessive compression, while ‘flow-sum’ ranks second, benefiting from additive aggregation. ‘Layer-mean’ and ‘layer-max’ demonstrate robust mid-level performance, avoiding biases introduced by explicit aggregation functions. Among all methods, *learned aggregation consistently outperforms others*, confirming its ability to preserve pretrained attention mechanisms while capturing complex semantic correlations.

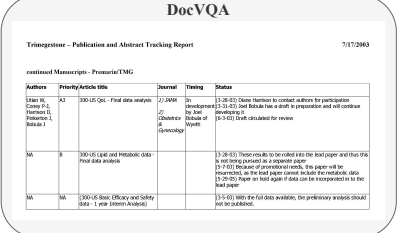
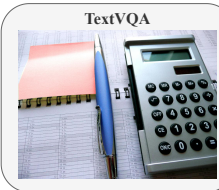
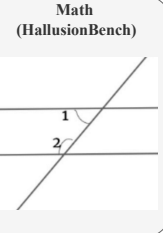
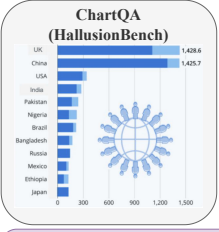
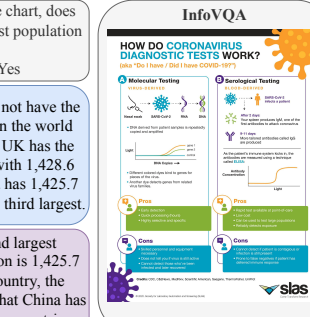
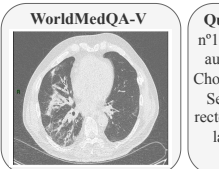
DocVQA	TextVQA	TextVQA	Math (HallusionBench)	Question:
				What is the heading of the table? Correct Answer: [continued manuscripts - premarin/tmg', 'continued Manuscripts - Prema...]
Llama-3.2: Trimegestone - Publication and Abstract Tracking Report	Llama-3.2: TextVQA	Lavender: continued Manuscripts - Prema.../TMG		Llama-3.2: No, angle 1 and angle 2 are not supplementary because they are not supplementary angles. They are corresponding angles. If two parallel lines are cut by a transversal, the corresponding angles are congruent.
Lavender: continued Manuscripts - Prema.../TMG	Lavender: off			Lavender: Yes, according to the parallel lines theorem, angle 1 + angle 2 = 180. This is because when two parallel lines are cut by a transversal, the corresponding angles are supplementary.
ChartQA (HallusionBench)	InfoVQA	InfoVQA	InfoVQA	Question:
				Is the right orange circle the same size as the left orange circle? Correct Answer: No. The right orange circle is larger than the left orange circle.
Lavender: Yes, according to the chart, China has the second largest population in the world. The chart shows that China's population is 1,425.7 million, which is significantly higher than the next closest country, the United States, with a population of 300 million. This indicates that China has a substantial lead in terms of population size compared to other countries.	Llama-3.2: No, China does not have the second largest population in the world according to the chart. The UK has the second largest population with 1,428.6 million people, while China has 1,425.7 million people, making it the third largest.	Llama-3.2: The orange circles on the left and right are the same size. Lavender: 93.	Llama-3.2: No, the right orange circle is significantly larger than the left orange circle. The right orange circle appears to be the largest circle in the image, while the left orange circle is relatively small compared to the surrounding gray circles.	
Lavender: off	Lavender: Q-1: Two Q-2: 4	Lavender: Q-1: Two Q-2: 3	Lavender: Q-1: Two Q-2: 4	Lavender: Who is the third in the list of most influential USA Olympians? Correct Answer: hope solo
WorldMedQA-V	Question:	Answer:	Answer:	Question:
	[Spanish] Pregunta vinculada a la imagen nº13 Mujer de 72 años con antecedentes de fibrilación auricular en tratamiento con anticoagulantes orales. Choices: A) Hernia complicada de pared abdominal B) Seroma postquirúrgico. C) Absceso en la vaina del recto anterior izquierdo del abdomen. D) Hematoma en la vaina del recto anterior izquierdo del abdomen.	Correct Answer: C.	Absceso en la vaina del recto anterior izquierdo del abdomen. Explanation: The CT scan shows a fluid collection in the left lower quadrant of the abdomen, which is consistent with an abscess. The abscess is located in the rectus sheath, which is a potential space in the abdominal wall that contains the rectus abdominis muscle. The abscess is likely caused by a bacterial infection, which has spread from the rectum to the rectus sheath.	Llama-3.2: Answer: C. Lavender: The correct answer is D. Hematoma in the anterior rectal sheath of the left abdomen. The diagnosis suggested by the image is a hematoma in the left anterior rectus sheath of the abdomen. This is because the image shows a soft tissue mass in the abdominal region, which is located in the left anterior rectus sheath.
	Choices: A) Hernia complicada de pared abdominal B) Seroma postquirúrgico. C) Absceso en la vaina del recto anterior izquierdo del abdomen. D) Hematoma en la vaina del recto anterior izquierdo del abdomen.	Correct Answer: D.		Llama-3.2: LeBron James. Lavender: Hope Solo.

Figure 18. Examples demonstrating Lavender’s enhanced fine-granularity vision alignment leading to improved accuracy on various VQA benchmarks. In the DocVQA example on the top-left, with a question about the title of a table, Llama-3.2 mistakenly extracts the section/page title at the top, which is also in bold, while Lavender correctly identifies the table title located next to the table. Similarly, more accurate visual understanding is directly observed in the two TextVQA examples in the second row. Impressively, the example from HallucinationBench demonstrates Lavender’s deep visual understanding of geometry, size, and spatial location, leading to robust anti-hallucination behaviour compared to the original Llama-3.2. In the ChartQA and two InfoVQA examples in the third row, Lavender exhibits its ability to recognise more detailed information, including relatively small elements within the graphs. In the WorldMedQA-V example, which is out-of-distribution, both Llama-3.2 and Lavender understand the question posed in a small language (Spanish) and answer in English. However, Llama-3.2 fails to provide the correct answer due to less accurate visual localization of the unhealthy region. It incorrectly identifies the region as the ‘rectus sheath,’ which surrounds the actual area of interest, leading to an incorrect response. In contrast, Lavender accurately locates the ‘soft tissue mass’, resulting in the correct answer.

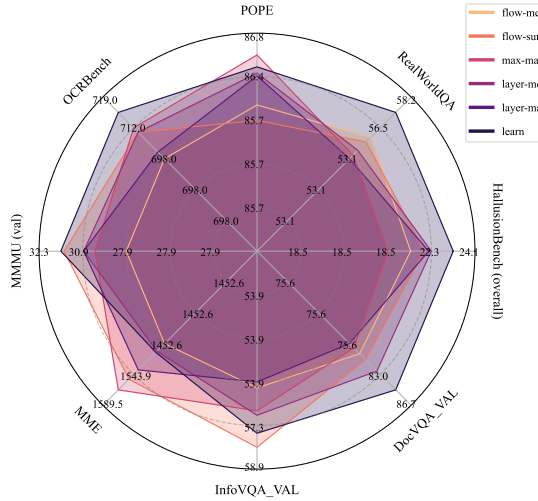


Figure 19. Comparison of aggregation functions on eight benchmarks. Evaluated using Lavender-Llama 3.2-11B fine-tuned on Flickr-1k for 20 epochs, using ‘exact match’ without an LLM judge.

Scalability of Aggregation Functions. We further assess the scalability of the proposed aggregation functions by comparing the eight benchmarks’ performance at different training lengths. The average results are shown in Figure 20, with detailed results for each individual benchmark provided in Figure 29. Despite the consistent overall ranking discussed earlier, the ‘learn’ aggregation strategy demonstrates the best scalability. Starting as the second worst at epoch 5, it climbs to the best-performing method by epoch 20. This behaviour can be understood in light of the limitations of manually designed aggregations, such as ‘flow-sum.’ While manual aggregations may initially reflect straightforward text-to-region correlations, like identifying colours in images, they are inherently suboptimal. These methods act as a shortcut, achieving good early performance but lacking scalability when encountering more complex text-to-region correlations. Learnable aggregation, in contrast, adapts to these complexities and scales effectively with additional training.

8.1.1. TRAINING RECIPES

Pretraining the Aligner Network. This work aims to enhance the alignment of pretrained VLMs, such as Llama-3.2, which are already knowledgeable. As discussed in Section 6, fully fine-tuning such VLMs with a secondary attention alignment objective and a small dataset can lead to catastrophic forgetting. The results in the first row of Figure 21 confirm this concern, showing drastic drops in performance across eight evaluated benchmarks after fully fine-tuning on a small dataset for 30 epochs. In contrast, the proposed pretraining strategy significantly mitigates this

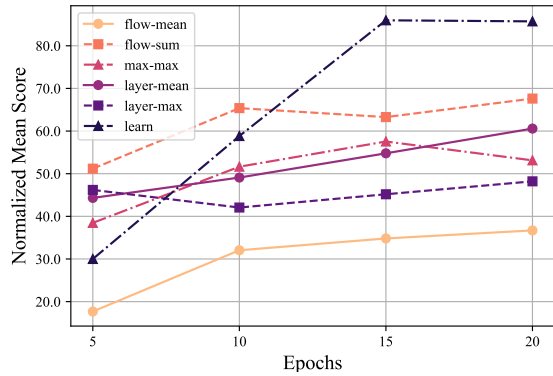


Figure 20. Mean performance across eight benchmarks over training epochs with various aggregation functions. The results are derived from Lavender-Llama 3.2-11B, fully fine-tuned on the Flickr-1k subset. Figure 29 provides detailed performance for each benchmark.

issue. The pretraining strategy involves pretraining only the Aligner Network for a certain number of epochs while keeping the VLM parameters frozen, before jointly updating all parameters. Results in Figure 21 show that pretraining for a short duration (less than one-third of the total epochs) is particularly effective overall. Notably, more challenging benchmarks that require deeper interaction between visual perception, complex reasoning, and domain knowledge, such as MMU and RealWorldQA, benefit more from longer pretraining.

Full Finetuning Versus LoRA. Comparing full finetuning with the LoRA finetuning strategy for Lavender, our main results with Llama-3.2 in Figure 15 (b) and Table 1 suggest that LoRA is generally more beneficial for the majority of benchmarks. However, we also observe that full finetuning outperforms LoRA with Lavender on a few more challenging benchmarks, such as MMU, MMStar, and RealWorldQA, which require deeper interactions between visual perception, complex reasoning, and domain knowledge. This observation is consistent with the results from the ablation study in Figure 21. Given that this work focuses on short finetuning overall, these findings suggest that *LoRA finetuning with Lavender offers better short-term benefits*. In contrast, *scaling Lavender with full finetuning may lead to deeper alignment and knowledge restructuring, potentially resulting in longer-term advantages*.

Choice of Layers to Align. We examine the choice of cross-attention layers to align with Lavender in the Llama 3.2-11B Vision Instruct model. This model comprises 40 layers in total, 8 of which are cross-attention layers integrated to process visual inputs, constituting one-fifth of the model’s layers. Figure 22 compares

Diffusion Instruction Tuning

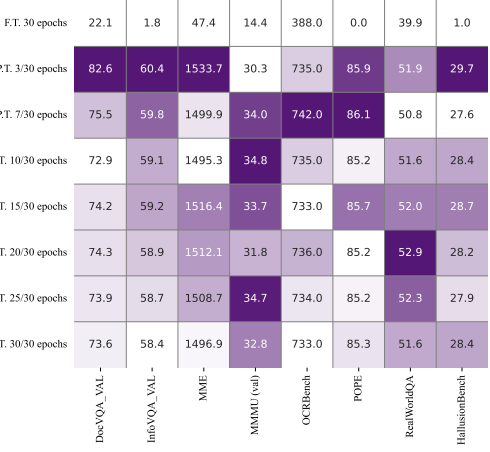


Figure 21. Fully fine-tuning (F.T.) leads to catastrophic forgetting, while short Aligner pretraining (P.T.) prevents this. Evaluated on eight benchmarks with Lavender-Llama 3.2-11B fine-tuned on Flickr-1k for 30 epochs.

the performance of four different subsets of the 8 cross-attention layers. While attending to the first, mid, or last subset shows shifted strengths on specific benchmarks—RealWorldQA/OCRBench, MMMU/POPE, and Hallucination, respectively—aligning all 8 layers proves to be the most effective overall. Therefore, this is the default strategy adopted in this work.

9. Failure Strategies

Despite the successful strategies presented earlier, we also tested the following approaches and found them to be less effective: 1) *Fully Finetuning Without Pretraining*. As shown in Figure 21, fully finetuning without pretraining often destabilises the model, while LoRA proves to be generally robust. We recommend starting with LoRA on small datasets as a reliable initial strategy for exploring Lavender, reserving full finetuning for scaling efforts and investigating emerging behaviours after deep alignment. 2) *Frequent Switching Between Training Strategies*. Given the varied performance of certain Lavender strategies, such as long fully finetuning or aligning subsets of cross-attention layers, we experimented with more complex staged training strategies. These involved switching between different strategies across epochs. However, frequent strategy changes harmed performance, likely due to the short overall training length. The model appeared to struggle with prioritizing objectives across strategies before stabilizing, leading to crashes. 3) *Mixing Extra Data*. In some cases, adding extra data did not improve performance. For example, as shown in Figure 27, mixing the OCRVQA dataset reduced overall performance. This suggests that OCRVQA may lead to overfitting more readily than other datasets tested.

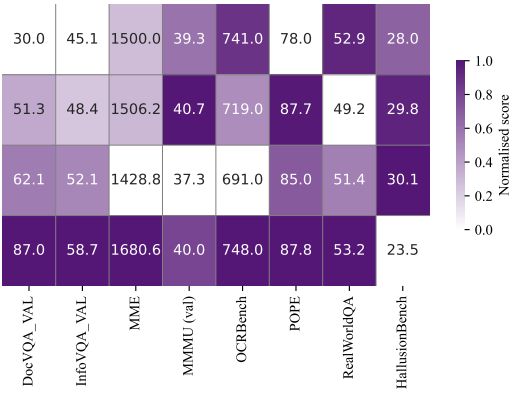


Figure 22. Aligning all eight cross-attention layers in Llama-3.2 with Lavender is most effective. This ablation study examines the impact of aligning subsets of the eight cross-attention layers {8, 13, 18, 23, 28, 33, 38} in Llama-3.2, denoted as ‘First 3/8,’ ‘Mid 4/8,’ ‘Last 4/8,’ and ‘All 8/8,’ as shown in each row. The results are derived from Lavender-Llama 3.2-11B, LoRA fine-tuned on the Flickr-1k subset for 30 epochs and evaluated on eight VLM benchmarks using ‘exact match’ without an LLM judge.

10. Limitation and Future Works

1) *Limited Compute*. Lavender was evaluated on datasets up to 0.13M samples, constrained by available compute resources. This is far smaller than the 5M–50M samples used by state-of-the-art models (approximately 38x to 384x larger). Figure 27 shows non-convergent scaling behaviour, suggesting that increasing dataset size and tuning duration could further boost performance. 2) *Exploring Higher-Resolution Diffusion Models*. In this work, Lavender uses Stable Diffusion v1.4 (Rombach et al., 2021). More advanced models, such as Stable Diffusion v2 (Rombach et al., 2022), could deliver higher-resolution, more precise attention maps but would demand memory beyond the capacity of this study. With further scaling and tuning, such approaches could become viable, marking an important direction for future research. 3) *More Accurate Attention Map Extraction*. This study focuses on demonstrating Lavender’s feasibility rather than optimising the quality of diffusion model attention maps, which already exhibit strong text-region alignment. Short inversion and diffusion steps produced per-word attention maps in 20 seconds per image on a single V100 GPU. While efficient, this method may limit accuracy for infrequent words (Jin et al., 2023). Future work could explore faster, more precise attention map estimation to further enhance performance. 4) *Improved Handling of Self-Attention-Only Models*. We demonstrate that Lavender can be applied to self-attention-only models such as MiniCPM-v-2.5 (based on Llama-3). However, further optimisation for these models remains under-explored due to limited resources. In particular, the advanced parallel atten-

tion mechanism—effective in the Llama-3.2 implementation of Lavender—warrants additional theoretical and empirical study to better translate between self- and cross-attention, benefiting the broader community.

11. Broad Impacts

Synergy Between Models: Building a Stronger Vision-Language Ecosystem. Lavender is a model-agnostic framework that requires no additional human annotations on existing data, making it broadly applicable for enhancing a wide range of VLMs. Given that text–vision alignment is central to most VLM tasks, our attention alignment approach is poised to benefit most downstream applications, as confirmed by extensive benchmark evaluations. Although primarily designed for cross-attention-equipped VLMs, early results show that Lavender also works with self-attention-only models, opening the door to converting widely available LLMs into effective VLMs without re-training. This capability unites the strengths of LLM and diffusion models into a more powerful multimodal expert.

Data Scarcity. Both the language and vision communities face looming data shortages, with paired vision–text datasets—the “crude oil” of VLM training—being particularly scarce. End-to-end training from scratch is resource-intensive and often impractical. Large-scale LLMs and DMs have been trained on multi-billion-level datasets, making it inefficient if their knowledge remains isolated. Lavender bridges these models using limited resources—requiring as little as a few thousand samples and one day of training on 8 Nvidia A10G GPUs—enabling small models (below 13B parameters) to perform on par with much larger models (over 50B parameters) across multiple benchmarks.

Data Privacy. By leveraging the extensive prior knowledge of diffusion models, Lavender aligns external VLMs with small, local datasets through automatic per-text attention map labelling. This approach is ideal for organisations with limited sensitive data and constrained computational resources, as it enables them to benefit from large-scale pretrained models while keeping data local.

VLM Attention Alignment with Other Vision Foundation Models. Lavender enhances text–vision correlation by directly aligning attention within LLM transformer layers. Although our current alignment objectives are derived from Stable Diffusion’s attention maps, the same methodology can be applied to other vision foundation models.

Alternative Multimodal Modalities Beyond Vision–Language. While our results focus on language and vision, the core idea of aligning cross-attention layers is broadly applicable. Potential applications include

text-to-audio alignment (Radford et al., 2023), sequence-to-structure tasks in protein generation (Jumper et al., 2021; Yang et al., 2023), and diverse biomedical applications (Tu et al., 2024; Yang et al., 2024) involving genomics, radiography, pathology, and mammography.

Attention Alignment as Vision Feedback in Reinforcement Learning. Our proposed attention alignment loss provides a scalable solution for vision feedback during the RL post-training phase. By leveraging the visual expertise encoded in image generation models, it eliminates the need for costly, fine-grained human annotations and mitigates bias in manual feedback. In effect, it replaces or augments traditional human visual feedback with “diffusion feedback”, streamlining the process, reducing training costs, and democratising access to advanced multimodal systems.

12. Conclusion

We have introduced Lavender, a method that leverages the precise text-region alignment of Diffusion Models to enhance Vision-Language Models (VLMs) through efficient supervised fine-tuning. Lavender enables significant performance improvements while remaining highly data-efficient and compute-friendly. Our findings highlight that Lavender effectively aligns VLM attention with Diffusion Models, improving robustness across diverse domains, including challenging and multilingual benchmarks. By incorporating techniques such as parallel attention and LoRA, Lavender balances attention alignment with the preservation of pretrained knowledge, ensuring consistent performance gains without catastrophic forgetting. This scalable, model-agnostic approach demonstrates the promising potential for advancing text–vision alignment in multimodal LLMs and lays the groundwork for future research into efficient fine-tuning and cross-modal alignment techniques.

References

- Abnar, S. and Zuidema, W. Quantifying attention flow in transformers. *arXiv preprint arXiv:2005.00928*, 2020.
- Agrawal, P., Antoniak, S., Hanna, E. B., Bout, B., Chaplot, D., Chudnovsky, J., Costa, D., Monicault, B. D., Garg, S., Gervet, T., Ghosh, S., Héliou, A., Jacob, P., Jiang, A. Q., Khandelwal, K., Lacroix, T., Lample, G., Casas, D. L., Lavril, T., Scao, T. L., Lo, A., Marshall, W., Martin, L., Mensch, A., Muddireddy, P., Nemychnikova, V., Pellat, M., Platen, P. V., Raghuraman, N., Rozière, B., Sablayrolles, A., Saulnier, L., Sauvestre, R., Shang, W., Soletskyi, R., Stewart, L., Stock, P., Studnia, J., Subramanian, S., Vaze, S., Wang, T., and Yang, S. Pixtral 12b, 2024. URL <https://arxiv.org/abs/2410.07073>.
- Alayrac, J.-B., Donahue, J., Luc, P., Miech, A., Barr, I., Hasson, Y., Lenc, K., Mensch, A., Millican, K., Reynolds, M., et al. Flamingo: a visual language model for few-shot learning. *Advances in Neural Information Processing Systems*, 35:23716–23736, 2022.
- Anthropic, A. The claude 3 model family: Opus, sonnet, haiku. *Claude-3 Model Card*, 1, 2024.
- Antol, S., Agrawal, A., Lu, J., Mitchell, M., Batra, D., Zitnick, C. L., and Parikh, D. Vqa: Visual question answering. In *Proceedings of the IEEE international conference on computer vision*, pp. 2425–2433, 2015.
- Bai, J., Bai, S., Chu, Y., Cui, Z., Dang, K., Deng, X., Fan, Y., Ge, W., Han, Y., Huang, F., Hui, B., Ji, L., Li, M., Lin, J., Lin, R., Liu, D., Liu, G., Lu, C., Lu, K., Ma, J., Men, R., Ren, X., Ren, X., Tan, C., Tan, S., Tu, J., Wang, P., Wang, S., Wang, W., Wu, S., Xu, B., Xu, J., Yang, A., Yang, H., Yang, J., Yang, S., Yao, Y., Yu, B., Yuan, H., Yuan, Z., Zhang, J., Zhang, X., Zhang, Y., Zhang, Z., Zhou, C., Zhou, J., Zhou, X., and Zhu, T. Qwen technical report, 2023. URL <https://arxiv.org/abs/2309.16609>.
- Brown, T., Mann, B., Ryder, N., Subbiah, M., Kaplan, J. D., Dhariwal, P., Neelakantan, A., Shyam, P., Sastry, G., Askell, A., et al. Language models are few-shot learners. *Advances in neural information processing systems*, 33: 1877–1901, 2020.
- Cha, J., Kang, W., Mun, J., and Roh, B. Honeybee: Locality-enhanced projector for multimodal llm. In *Proceedings of the IEEE/CVF Conference on Computer Vision and Pattern Recognition*, pp. 13817–13827, 2024.
- Chen, G., Liu, X., Wang, G., Zhang, K., Torr, P. H., Zhang, X.-P., and Tang, Y. Tem-adapter: Adapting image-text pretraining for video question answer. In *Proceedings of the IEEE/CVF International Conference on Computer Vision*, pp. 13945–13955, 2023.
- Chen, L., Li, J., Dong, X., Zhang, P., Zang, Y., Chen, Z., Duan, H., Wang, J., Qiao, Y., Lin, D., et al. Are we on the right way for evaluating large vision-language models? *arXiv preprint arXiv:2403.20330*, 2024a.
- Chen, L., Li, J., Dong, X., Zhang, P., He, C., Wang, J., Zhao, F., and Lin, D. Sharegpt4v: Improving large multi-modal models with better captions. In *European Conference on Computer Vision*, pp. 370–387. Springer, 2025a.
- Chen, X., Fang, H., Lin, T.-Y., Vedantam, R., Gupta, S., Dollár, P., and Zitnick, C. L. Microsoft coco captions: Data collection and evaluation server. *arXiv preprint arXiv:1504.00325*, 2015.
- Chen, X., Wu, Z., Liu, X., Pan, Z., Liu, W., Xie, Z., Yu, X., and Ruan, C. Janus-pro: Unified multimodal understanding and generation with data and model scaling, 2025b. URL <https://arxiv.org/abs/2501.17811>.
- Chen, Z., Wu, J., Wang, W., Su, W., Chen, G., Xing, S., Zhong, M., Zhang, Q., Zhu, X., Lu, L., et al. Internvl: Scaling up vision foundation models and aligning for generic visual-linguistic tasks. In *Proceedings of the IEEE/CVF Conference on Computer Vision and Pattern Recognition*, pp. 24185–24198, 2024b.
- Chowdhery, A., Narang, S., Devlin, J., Bosma, M., Mishra, G., Roberts, A., Barham, P., Chung, H. W., Sutton, C., Gehrmann, S., et al. Palm: Scaling language modeling with pathways. *Journal of Machine Learning Research*, 24(240):1–113, 2023.
- Covert, I., Sun, T., Zou, J., and Hashimoto, T. Locality alignment improves vision-language models. *arXiv preprint arXiv:2410.11087*, 2024.
- Dai, W., Li, J., Li, D., Tiong, A. M. H., Zhao, J., Wang, W., Li, B., Fung, P., and Hoi, S. Instructblip: Towards general-purpose vision-language models with instruction tuning, 2023. URL <https://arxiv.org/abs/2305.06500>.
- DeepSeek-AI, Liu, A., Feng, B., Xue, B., Wang, B., Wu, B., Lu, C., Zhao, C., Deng, C., Zhang, C., Ruan, C., Dai, D., Guo, D., Yang, D., Chen, D., Ji, D., Li, E., Lin, F., Dai, F., Luo, F., Hao, G., Chen, G., Li, G., Zhang, H., Bao, H., Xu, H., Wang, H., Zhang, H., Ding, H., Xin, H., Gao, H., Li, H., Qu, H., Cai, J. L., Liang, J., Guo, J., Ni, J., Li, J., Wang, J., Chen, J., Chen, J., Yuan, J., Qiu, J., Li, J., Song, J., Dong, K., Hu, K., Gao, K., Guan, K., Huang, K., Yu, K., Wang, L., Zhang, L., Xu, L., Xia, L., Zhao, L., Wang, L., Zhang, L., Li, M., Wang, M., Zhang, M., Zhang, M., Tang, M., Li, M., Tian, N., Huang, P., Wang, P., Zhang, P., Wang, Q., Zhu, Q., Chen, Q., Du, Q., Chen, R. J., Jin, R. L., Ge, R., Zhang, R., Pan, R., Wang, R., Xu, R., Zhang, R., Chen, R., Li, S. S., Lu, S., Zhou, S.,

- Chen, S., Wu, S., Ye, S., Ye, S., Ma, S., Wang, S., Zhou, S., Yu, S., Zhou, S., Pan, S., Wang, T., Yun, T., Pei, T., Sun, T., Xiao, W. L., Zeng, W., Zhao, W., An, W., Liu, W., Liang, W., Gao, W., Yu, W., Zhang, W., Li, X. Q., Jin, X., Wang, X., Bi, X., Liu, X., Wang, X., Shen, X., Chen, X., Zhang, X., Chen, X., Nie, X., Sun, X., Wang, X., Cheng, X., Liu, X., Xie, X., Liu, X., Yu, X., Song, X., Shan, X., Zhou, X., Yang, X., Li, X., Su, X., Lin, X., Li, Y. K., Wang, Y. Q., Wei, Y. X., Zhu, Y. X., Zhang, Y., Xu, Y., Xu, Y., Huang, Y., Li, Y., Zhao, Y., Sun, Y., Li, Y., Wang, Y., Yu, Y., Zheng, Y., Zhang, Y., Shi, Y., Xiong, Y., He, Y., Tang, Y., Piao, Y., Wang, Y., Tan, Y., Ma, Y., Liu, Y., Guo, Y., Wu, Y., Ou, Y., Zhu, Y., Wang, Y., Gong, Y., Zou, Y., He, Y., Zha, Y., Xiong, Y., Ma, Y., Yan, Y., Luo, Y., You, Y., Liu, Y., Zhou, Y., Wu, Z. F., Ren, Z. Z., Ren, Z., Sha, Z., Fu, Z., Xu, Z., Huang, Z., Zhang, Z., Xie, Z., Zhang, Z., Hao, Z., Gou, Z., Ma, Z., Yan, Z., Shao, Z., Xu, Z., Wu, Z., Zhang, Z., Li, Z., Gu, Z., Zhu, Z., Liu, Z., Li, Z., Xie, Z., Song, Z., Gao, Z., and Pan, Z. Deepseek-v3 technical report, 2024. URL <https://arxiv.org/abs/2412.19437>.
- Deitke, M., Clark, C., Lee, S., Tripathi, R., Yang, Y., Park, J. S., Salehi, M., Muennighoff, N., Lo, K., Soldaini, L., et al. Molmo and pixmo: Open weights and open data for state-of-the-art multimodal models. *arXiv preprint arXiv:2409.17146*, 2024.
- Dosovitskiy, A. An image is worth 16x16 words: Transformers for image recognition at scale. *arXiv preprint arXiv:2010.11929*, 2020.
- Duan, H., Yang, J., Qiao, Y., Fang, X., Chen, L., Liu, Y., Dong, X., Zang, Y., Zhang, P., Wang, J., et al. Vlmevalkit: An open-source toolkit for evaluating large multi-modality models. In *Proceedings of the 32nd ACM International Conference on Multimedia*, pp. 11198–11201, 2024.
- Dubey, A., Jauhri, A., Pandey, A., Kadian, A., Al-Dahle, A., Letman, A., Mathur, A., Schelten, A., Yang, A., Fan, A., et al. The llama 3 herd of models. *arXiv preprint arXiv:2407.21783*, 2024.
- Fu, C., Chen, P., Shen, Y., Qin, Y., Zhang, M., Lin, X., Qiu, Z., Lin, W., Yang, J., Zheng, X., et al. MME: A comprehensive evaluation benchmark for multimodal large language models. *arXiv:2306.13394*, 2023.
- Gao, P., Han, J., Zhang, R., Lin, Z., Geng, S., Zhou, A., Zhang, W., Lu, P., He, C., Yue, X., et al. Llama-adapter v2: Parameter-efficient visual instruction model. *arXiv preprint arXiv:2304.15010*, 2023.
- Gurari, D., Li, Q., Stangl, A. J., Guo, A., Lin, C., Grauman, K., Luo, J., and Bigham, J. P. Vizwiz grand challenge: Answering visual questions from blind people. In *Proceedings of the IEEE conference on computer vision and pattern recognition*, pp. 3608–3617, 2018.
- Hernandez, J., Villegas, R., and Ordóñez, V. Generative visual instruction tuning. *arXiv preprint arXiv:2406.11262*, 2024.
- Hertz, A., Mokady, R., Tenenbaum, J., Aberman, K., Pritch, Y., and Cohen-Or, D. Prompt-to-prompt image editing with cross attention control. 2022.
- Hu, J., Shen, L., and Sun, G. Squeeze-and-excitation networks. In *Proceedings of the IEEE conference on computer vision and pattern recognition*, pp. 7132–7141, 2018.
- Huang, X., Wang, J., Tang, Y., Zhang, Z., Hu, H., Lu, J., Wang, L., and Liu, Z. Segment and caption anything. In *Proceedings of the IEEE/CVF Conference on Computer Vision and Pattern Recognition*, pp. 13405–13417, 2024.
- Jaegle, A., Gimeno, F., Brock, A., Vinyals, O., Zisserman, A., and Carreira, J. Perceiver: General perception with iterative attention. In *International conference on machine learning*, pp. 4651–4664. PMLR, 2021.
- Jiang, D., Liu, Y., Liu, S., Zhao, J., Zhang, H., Gao, Z., Zhang, X., Li, J., and Xiong, H. From clip to dino: Visual encoders shout in multi-modal large language models. *arXiv preprint arXiv:2310.08825*, 2023.
- Jin, C., Tanno, R., Saseendran, A., Diethe, T., and Teare, P. An image is worth multiple words: Learning object level concepts using multi-concept prompt learning. *arXiv preprint arXiv:2310.12274*, 2023.
- Jumper, J., Evans, R., Pritzel, A., Green, T., Figurnov, M., Ronneberger, O., Tunyasuvunakool, K., Bates, R., Žídek, A., Potapenko, A., et al. Highly accurate protein structure prediction with alphafold. *nature*, 596(7873):583–589, 2021.
- Kar, O. F., Tonioni, A., Poklukar, P., Kulshrestha, A., Zamir, A., and Tombari, F. Brave: Broadening the visual encoding of vision-language models. In *European Conference on Computer Vision*, pp. 113–132. Springer, 2025.
- Karamcheti, S., Nair, S., Balakrishna, A., Liang, P., Kollar, T., and Sadigh, D. Prismatic vlms: Investigating the design space of visually-conditioned language models. *arXiv preprint arXiv:2402.07865*, 2024.
- Kembhavi, A., Salvato, M., Kolve, E., Seo, M., Hajishirzi, H., and Farhadi, A. A diagram is worth a dozen images. In *Computer Vision–ECCV 2016: 14th European Conference, Amsterdam, The Netherlands, October 11–14, 2016, Proceedings, Part IV 14*, pp. 235–251. Springer, 2016.

- Kiela, D., Firooz, H., Mohan, A., Goswami, V., Singh, A., Ringshia, P., and Testuggine, D. The hateful memes challenge: Detecting hate speech in multimodal memes. *Advances in neural information processing systems*, 33: 2611–2624, 2020.
- Koh, J. Y., Fried, D., and Salakhutdinov, R. R. Generating images with multimodal language models. *Advances in Neural Information Processing Systems*, 36, 2024.
- Li, B., Wang, R., Wang, G., Ge, Y., Ge, Y., and Shan, Y. Seed-Bench: Benchmarking multimodal llms with generative comprehension. *arXiv:2307.16125*, 2023a.
- Li, B., Zhang, Y., Guo, D., Zhang, R., Li, F., Zhang, H., Zhang, K., Zhang, P., Li, Y., Liu, Z., et al. Llava-onevision: Easy visual task transfer. *arXiv preprint arXiv:2408.03326*, 2024.
- Li, J., Li, D., Xiong, C., and Hoi, S. Blip: Bootstrapping language-image pre-training for unified vision-language understanding and generation. In *International conference on machine learning*, pp. 12888–12900. PMLR, 2022.
- Li, J., Li, D., Savarese, S., and Hoi, S. Blip-2: Bootstrapping language-image pre-training with frozen image encoders and large language models. In *International conference on machine learning*, pp. 19730–19742. PMLR, 2023b.
- Li, Y., Du, Y., Zhou, K., Wang, J., Zhao, W. X., and Wen, J.-R. Evaluating object hallucination in large vision-language models. *arXiv:2305.10355*, 2023c.
- Lin, Z., Wang, Y., and Tang, Z. Training-free open-ended object detection and segmentation via attention as prompts. *arXiv preprint arXiv:2410.05963*, 2024.
- Liu, F., Guan, T., Li, Z., Chen, L., Yacoob, Y., Manocha, D., and Zhou, T. HallusionBench: You see what you think? or you think what you see? an image-context reasoning benchmark challenging for gpt-4v (ision), llava-1.5, and other multi-modality models. *arXiv:2310.14566*, 2023a.
- Liu, H., Li, C., Li, Y., and Lee, Y. J. Improved baselines with visual instruction tuning. In *Proceedings of the IEEE/CVF Conference on Computer Vision and Pattern Recognition*, pp. 26296–26306, 2024a.
- Liu, H., Li, C., Li, Y., Li, B., Zhang, Y., Shen, S., and Lee, Y. J. Llava-next: Improved reasoning, ocr, and world knowledge, January 2024b. URL <https://llava-vl.github.io/blog/2024-01-30-llava-next/>.
- Liu, H., Li, C., Wu, Q., and Lee, Y. J. Visual instruction tuning. *Advances in neural information processing systems*, 36, 2024c.
- Liu, Y., Duan, H., Zhang, Y., Li, B., Zhang, S., Zhao, W., Yuan, Y., Wang, J., He, C., Liu, Z., Chen, K., and Lin, D. MMBench: Is your multi-modal model an all-around player? *arXiv:2307.06281*, 2023b.
- Liu, Y., Li, Z., Li, H., Yu, W., Huang, M., Peng, D., Liu, M., Chen, M., Li, C., and Jin, L. On the hidden mystery of ocr in large multimodal models. *Technical Report*, 2023c.
- Liu, Y., Zhang, C., Wang, Y., Wang, J., Yang, Y., and Tang, Y. Universal segmentation at arbitrary granularity with language instruction. In *Proceedings of the IEEE/CVF Conference on Computer Vision and Pattern Recognition*, pp. 3459–3469, 2024d.
- Longpre, S., Hou, L., Vu, T., Webson, A., Chung, H. W., Tay, Y., Zhou, D., Le, Q. V., Zoph, B., Wei, J., et al. The flan collection: Designing data and methods for effective instruction tuning. In *International Conference on Machine Learning*, pp. 22631–22648. PMLR, 2023.
- Lu, J., Clark, C., Lee, S., Zhang, Z., Khosla, S., Marten, R., Hoiem, D., and Kembhavi, A. Unified-io 2: Scaling autoregressive multimodal models with vision language audio and action. In *Proceedings of the IEEE/CVF Conference on Computer Vision and Pattern Recognition*, pp. 26439–26455, 2024.
- Marino, K., Rastegari, M., Farhadi, A., and Mottaghi, R. Ok-vqa: A visual question answering benchmark requiring external knowledge. In *Proceedings of the IEEE/cvf conference on computer vision and pattern recognition*, pp. 3195–3204, 2019.
- Masry, A., Long, D. X., Tan, J. Q., Joty, S., and Hoque, E. ChartQA: A benchmark for question answering about charts with visual and logical reasoning. *arXiv:2203.10244*, 2022.
- Mathew, M., Karatzas, D., and Jawahar, C. V. DocVQA: A dataset for vqa on document images. In *WACV*, 2021.
- Mathew, M., Bagal, V., Tito, R., Karatzas, D., Valveny, E., and Jawahar, C. Infographicvqa. In *Proceedings of the IEEE/CVF Winter Conference on Applications of Computer Vision*, pp. 1697–1706, 2022.
- Matos, J., Chen, S., Placino, S., Li, Y., Pardo, J. C. C., Idan, D., Tohyama, T., Restrepo, D., Nakayama, L. F., Pascual-Leone, J. M., et al. Worldmedqa-v: a multilingual, multimodal medical examination dataset for multimodal language models evaluation. *arXiv preprint arXiv:2410.12722*, 2024.
- Mishra, A., Shekhar, S., Singh, A. K., and Chakraborty, A. Ocr-vqa: Visual question answering by reading text in images. In *2019 international conference on document analysis and recognition (ICDAR)*, pp. 947–952. IEEE, 2019.

- Mokady, R., Hertz, A., Aberman, K., Pritch, Y., and Cohen-Or, D. Null-text inversion for editing real images using guided diffusion models, 2022. URL <https://arxiv.org/abs/2211.09794>.
- OpenAI. GPT-4 technical report. *arXiv preprint arXiv:2303.08774*, 2023.
- OpenAI. GPT-4o mini system card, 2024. URL <https://openai.com>.
- Ouyang, L., Wu, J., Jiang, X., Almeida, D., Wainwright, C., Mishkin, P., Zhang, C., Agarwal, S., Slama, K., Ray, A., et al. Training language models to follow instructions with human feedback. *Advances in neural information processing systems*, 35:27730–27744, 2022.
- Radford, A., Kim, J. W., Xu, T., Brockman, G., McLeavey, C., and Sutskever, I. Robust speech recognition via large-scale weak supervision. In *International conference on machine learning*, pp. 28492–28518. PMLR, 2023.
- Rombach, R., Blattmann, A., Lorenz, D., Esser, P., and Ommer, B. High-resolution image synthesis with latent diffusion models, 2021.
- Rombach, R., Blattmann, A., Lorenz, D., Esser, P., and Ommer, B. High-resolution image synthesis with latent diffusion models. In *Proceedings of the IEEE/CVF Conference on Computer Vision and Pattern Recognition (CVPR)*, pp. 10684–10695, June 2022.
- Saikh, T., Ghosal, T., Mittal, A., Ekbal, A., and Bhattacharyya, P. ScienceQA: A novel resource for question answering on scholarly articles. *International Journal on Digital Libraries*, 2022.
- Schuhmann, C., Beaumont, R., Vencu, R., Gordon, C., Wightman, R., Cherti, M., Coombes, T., Katta, A., Mullis, C., Wortsman, M., et al. Laion-5b: An open large-scale dataset for training next generation image-text models. *Advances in Neural Information Processing Systems*, 35: 25278–25294, 2022.
- Shi, M., Liu, F., Wang, S., Liao, S., Radhakrishnan, S., Huang, D.-A., Yin, H., Sapra, K., Yacoob, Y., Shi, H., et al. Eagle: Exploring the design space for multimodal llms with mixture of encoders. *arXiv preprint arXiv:2408.15998*, 2024.
- Shi, W., Han, X., Zhou, C., Liang, W., Lin, X. V., Zettlemoyer, L., and Yu, L. Lmfusion: Adapting pretrained language models for multimodal generation, 2025. URL <https://arxiv.org/abs/2412.15188>.
- Singh, A., Natarajan, V., Shah, M., Jiang, Y., Chen, X., Batra, D., Parikh, D., and Rohrbach, M. Towards VQA models that can read. In *Proceedings of the IEEE/CVF conference on computer vision and pattern recognition*, pp. 8317–8326, 2019.
- Team, G. Gemini 1.5: Unlocking multimodal understanding across millions of tokens of context. *arXiv preprint arXiv:2403.05530*, 2024.
- Tong, S., Brown, E., Wu, P., Woo, S., Middepogu, M., Akula, S. C., Yang, J., Yang, S., Iyer, A., Pan, X., Wang, A., Fergus, R., LeCun, Y., and Xie, S. Cambrian-1: A Fully Open, Vision-Centric Exploration of Multimodal LLMs. *arXiv preprint arXiv:2406.16860*, 2024a.
- Tong, S., Fan, D., Zhu, J., Xiong, Y., Chen, X., Sinha, K., Rabbat, M., LeCun, Y., Xie, S., and Liu, Z. Metamorph: Multimodal understanding and generation via instruction tuning. *arXiv preprint arXiv:2412.14164*, 2024b.
- Tong, S., Liu, Z., Zhai, Y., Ma, Y., LeCun, Y., and Xie, S. Eyes wide shut? exploring the visual shortcomings of multimodal llms. In *Proceedings of the IEEE/CVF Conference on Computer Vision and Pattern Recognition*, pp. 9568–9578, 2024c.
- Tu, T., Azizi, S., Driess, D., Schaeckermann, M., Amin, M., Chang, P.-C., Carroll, A., Lau, C., Tanno, R., Ktena, I., et al. Towards generalist biomedical ai. *NEJM AI*, 1(3): A1oa2300138, 2024.
- Vaswani, A. Attention is all you need. *Advances in Neural Information Processing Systems*, 2017.
- Wang, P., Bai, S., Tan, S., Wang, S., Fan, Z., Bai, J., Chen, K., Liu, X., Wang, J., Ge, W., et al. Qwen2-vl: Enhancing vision-language model’s perception of the world at any resolution. *arXiv preprint arXiv:2409.12191*, 2024a.
- Wang, W., Chen, Z., Chen, X., Wu, J., Zhu, X., Zeng, G., Luo, P., Lu, T., Zhou, J., Qiao, Y., et al. Visionllm: Large language model is also an open-ended decoder for vision-centric tasks. *Advances in Neural Information Processing Systems*, 36, 2024b.
- Wang, W., Sun, Q., Zhang, F., Tang, Y., Liu, J., and Wang, X. Diffusion feedback helps clip see better. *arXiv preprint arXiv:2407.20171*, 2024c.
- x.ai. Grok-1.5 vision preview. URL <https://x.ai/blog/grok-1.5v>.
- Yang, L., Xu, S., Sellergren, A., Kohlberger, T., Zhou, Y., Ktena, I., Kiraly, A., Ahmed, F., Hormozdiari, F., Jaroensri, T., et al. Advancing multimodal medical capabilities of gemini. *arXiv preprint arXiv:2405.03162*, 2024.
- Yang, Z., Zeng, X., Zhao, Y., and Chen, R. AlphaFold2 and its applications in the fields of biology and medicine. *Sigmal Transduction and Targeted Therapy*, 8(1):115, 2023.

Yao, Y., Yu, T., Zhang, A., Wang, C., Cui, J., Zhu, H., Cai, T., Li, H., Zhao, W., He, Z., Chen, Q., Zhou, H., Zou, Z., Zhang, H., Hu, S., Zheng, Z., Zhou, J., Cai, J., Han, X., Zeng, G., Li, D., Liu, Z., and Sun, M. Minicpm-v: A gpt-4v level mllm on your phone. *arXiv preprint 2408.01800*, 2024.

You, H., Zhang, H., Gan, Z., Du, X., Zhang, B., Wang, Z., Cao, L., Chang, S.-F., and Yang, Y. Ferret: Refer and ground anything anywhere at any granularity. *arXiv preprint arXiv:2310.07704*, 2023.

Young, P., Lai, A., Hodosh, M., and Hockenmaier, J. From image descriptions to visual denotations: New similarity metrics for semantic inference over event descriptions. *Transactions of the Association for Computational Linguistics*, 2:67–78, 2014.

Yu, T., Zhang, H., Yao, Y., Dang, Y., Chen, D., Lu, X., Cui, G., He, T., Liu, Z., Chua, T.-S., and Sun, M. Rlaif-v: Aligning mllms through open-source ai feedback for super gpt-4v trustworthiness. *arXiv preprint arXiv:2405.17220*, 2024.

Yue, X., Ni, Y., Zhang, K., Zheng, T., Liu, R., Zhang, G., Stevens, S., Jiang, D., Ren, W., Sun, Y., et al. MMMU: A massive multi-discipline multimodal understanding and reasoning benchmark for expert AGI. In *CVPR*, 2024.

Zheng, L., Chiang, W.-L., Sheng, Y., Zhuang, S., Wu, Z., Zhuang, Y., Lin, Z., Li, Z., Li, D., Xing, E., et al. Judging llm-as-a-judge with mt-bench and chatbot arena. *Advances in Neural Information Processing Systems*, 36: 46595–46623, 2023.

Zhou, C., Yu, L., Babu, A., Tirumala, K., Yasunaga, M., Shamis, L., Kahn, J., Ma, X., Zettlemoyer, L., and Levy, O. Transfusion: Predict the next token and diffuse images with one multi-modal model. *arXiv preprint arXiv:2408.11039*, 2024.

Zhu, D., Chen, J., Shen, X., Li, X., and Elhoseiny, M. Minigpt-4: Enhancing vision-language understanding with advanced large language models. *arXiv preprint arXiv:2304.10592*, 2023.

Zhu, W., Hessel, J., Awadalla, A., Gadre, S. Y., Dodge, J., Fang, A., Yu, Y., Schmidt, L., Wang, W. Y., and Choi, Y. Multimodal c4: An open, billion-scale corpus of images interleaved with text. *Advances in Neural Information Processing Systems*, 36, 2024.

Zong, Z., Ma, B., Shen, D., Song, G., Shao, H., Jiang, D., Li, H., and Liu, Y. Mova: Adapting mixture of vision experts to multimodal context. *arXiv preprint arXiv:2404.13046*, 2024.

Appendix Table of Contents

Appendix A - Full Pseudo Code of Diffusion Instruction Tuning	24
Appendix B - Bayesian Justification for DM Attention Proximity	24
Appendix C - Justification of the Attention Alignment Loss	26
Appendix D - Additional Details on Attention Flow in Vision-Language Models	28
Appendix E - Appropriate Rearrangement and Reconstruction Matter	28
<i>Figure 23: Reconstruction Tiles</i>	29
<i>Figure 24: Reconstruction Debug</i>	29
Appendix F - Extended Supplementary Results	30
F.1. Extra Proof of Concept Results	30
<i>Figure 25: Entropy Histograms</i>	30
<i>Figure 26: Visual Attention Verification</i>	31
F.2. Full Scaling Results	30
<i>Figure 27: Scaling Mean Performance</i>	33
<i>Figure 28: Scaling Across Benchmarks</i>	34
F.3. Extra Ablation Results	32
<i>Figure 29: Ablation Aggregation Functions</i>	35
F.4. Extra Visual Results	32
<i>Table 2: WorldMedQA-V Example Results</i>	36
<i>Table 3: Failure Case Analysis on the MME Benchmark</i>	37
<i>Figure 30: Visual Alignment Examples</i>	38

A. Full Pseudo Code of Diffusion Instruction Tuning [Back to Contents]

This section expands on Algorithm 1: *Algorithm 1*, as introduced in the main paper.

Algorithm 2 Diffusion Instruction Tuning (Full Version)

Require: Dataset $D = \{(x^{(i)}, y_q^{(i)}, y_l^{(i)})\}_{i=1}^N$, where $y_q^{(i)}$ is textual input (e.g. a question) and $y_l^{(i)}$ is the target textual output. Pretrained DM parameters θ_D , pretrained VLM parameters θ . Scaling factor $\lambda > 0$, learning rate η .

Ensure: Fine-tuned VLM parameters θ

- 1: **Stage 1: Preprocessing (Run Once)**
- 2: For each data point $(x^{(i)}, y^{(i)})$ in D :
- 3: Use the pretrained DM (θ_D fixed) to compute $p_{\text{DM}}(a | x^{(i)}, y^{(i)}; \theta_D)$
- 4: Store these attention distributions: $A_{\text{DM}}^{(i)} \leftarrow p_{\text{DM}}(a | x^{(i)}, y^{(i)}; \theta_D)$
- 5: After this, we have a DM-derived attention target for each data point, which will remain fixed during fine-tuning.
- 6: **Stage 2: Fine-Tuning the VLM**
- 7: Initialise θ from a pretrained VLM.
- 8: Set a learning rate η and define maximum training steps or convergence criteria.
- 9: **repeat**
- 10: Sample a mini-batch $B \subseteq D$ of size m
- 11: $L_{\text{VLM}}(\theta) \leftarrow 0$, $L_{\text{att}}(\theta) \leftarrow 0$
- 12: **for** $(x^{(j)}, y^{(j)}, y_q^{(j)}, y_l^{(j)})$ in B **do**
- 13: Compute $p_{\text{VLM}}(a | x^{(j)}, y^{(j)}; \theta)$ by aggregating attention heads/layers of the VLM cross-/self-attention (see Section 4)
- 14: $\delta^{(j)}(\theta) \leftarrow \text{Aligner}(p_{\text{VLM}}(a | x^{(j)}, y^{(j)}; \theta)) - A_{\text{DM}}^{(j)}$
- 15: Compute task loss: $L_{\text{VLM}}(\theta) += -\log p(y_l^{(j)} | x^{(j)}, y_q^{(j)}; \theta)$
- 16: Compute attention alignment loss: $L_{\text{att}}(\theta) += \|\delta^{(j)}(\theta)\|^2$
- 17: **end for**
- 18: Form total loss: $L_{\text{total}}(\theta) = L_{\text{VLM}}(\theta) + \lambda L_{\text{att}}(\theta)$
- 19: Update parameters: $\theta \leftarrow \theta - \eta \nabla_{\theta} L_{\text{total}}(\theta)$
- 20: Optionally, apply LoRA or other optimization tricks if desired.
- 21: **until** convergence (e.g., validation metric plateaus or max steps reached)
- 22: **Output:** The fine-tuned VLM parameters θ .

B. Bayesian Justification for DM Attention Proximity [Back to Contents]

This section expands on Section 3.3: *Bayesian Derivation*, as discussed in the main paper. In this section, we provide a detailed Bayesian justification for our assumption that the DM’s attention distribution $p_{\text{DM}}(a | x, y; \theta_D)$ is closer to the optimal posterior attention distribution $p^*(a | x, y)$ than the VLM’s attention distribution $p_{\text{VLM}}(a | x, y; \theta)$.

Optimal Posterior Attention Distribution. We define the *ideal* attention distribution as the one that minimizes the VLM’s next-token prediction loss:

$$p^*(a | x, y) = \arg \min_{a \in \mathcal{R}^d} \mathbb{E}_{(x, y) \sim \mathcal{D}} \mathcal{L}_{\text{VLM}}(x, y, \theta), \quad (18)$$

where \mathcal{D} is the data distribution and \mathcal{L}_{VLM} is the loss function of the vision-language model. We assume that the DM’s attention distribution is closer to this ideal attention than the VLM’s, and in the following sections, we analyze this claim using Bayesian modelling and statistical comparisons.

B.1. Modelling Attention Distributions as Posteriors

We model the attention distributions in both the DM and the VLM as posterior probabilities over the attention a given the inputs and model parameters. For consistency, we consider the joint distributions and apply Bayes’ theorem.

Diffusion Model (DM): The DM is trained to generate an image x conditioned on text y by modelling the distribution $p_{\text{DM}}(x | y; \theta_D)$. We can express the attention mechanism in the DM as contributing to this distribution via:

$$p_{\text{DM}}(x \mid y; \theta_D) = \int p_{\text{DM}}(x \mid y, a; \theta_D) p_{\text{DM}}(a \mid y; \theta_D) da. \quad (19)$$

Applying Bayes' theorem, the posterior over attention a given x and y is:

$$p_{\text{DM}}(a \mid x, y; \theta_D) = \frac{p_{\text{DM}}(x \mid y, a; \theta_D) p_{\text{DM}}(a \mid y; \theta_D)}{p_{\text{DM}}(x \mid y; \theta_D)}. \quad (20)$$

Vision-Language Model (VLM): Similarly, for the VLM, which generates textual output y_l given an image x and textual input y_q , the attention mechanism influences the distribution $p_{\text{VLM}}(y_l \mid x, y_q; \theta)$:

$$p_{\text{VLM}}(y_l \mid x, y_q; \theta) = \int p_{\text{VLM}}(y_l \mid x, y_q, a; \theta) p_{\text{VLM}}(a \mid x, y_q; \theta) da. \quad (21)$$

The posterior over attention a is then:

$$p_{\text{VLM}}(a \mid x, y_q, y_l; \theta) = \frac{p_{\text{VLM}}(y_l \mid x, y_q, a; \theta) p_{\text{VLM}}(a \mid x, y_q; \theta)}{p_{\text{VLM}}(y_l \mid x, y_q; \theta)}. \quad (22)$$

B.2. Differences in Likelihood Functions

The key distinction arises from the likelihood functions:

- **DM Likelihood** $p_{\text{DM}}(x \mid y, a; \theta_D)$: The DM must reconstruct the image x accurately, which requires precise alignment between textual tokens and visual features. The attention a plays a critical role in ensuring that each part of the text y correctly influences the corresponding visual content in x .
- **VLM Likelihood** $p_{\text{VLM}}(y_l \mid x, y_q, a; \theta)$: The VLM generates text y_l based on the image x and input text y_q . While attention a aids in focusing on relevant visual regions, the text generation process can often rely on higher-level visual features and may not require as fine-grained vision-text alignment as the DM.

B.3. Entropy and Concentration of Attention Distributions

Due to the DM's need for precise image reconstruction, its attention distribution $p_{\text{DM}}(a \mid x, y; \theta_D)$ is expected to be more concentrated around the ideal attention $p^*(a \mid x, y)$. This can be quantified by the entropy H of the attention distributions:

$$H(p_{\text{DM}}(a \mid x, y; \theta_D)) < H(p_{\text{VLM}}(a \mid x, y_q; \theta)). \quad (23)$$

A lower entropy indicates that the DM's attention distribution is more peaked and thus closer to $p^*(a \mid x, y)$, whereas the VLM's higher entropy reflects a more diffuse attention distribution. **This is consistent with our empirical observations in Figure 3 and section 7.1.**

B.4. KL Divergence to the Ideal Attention

We can formalise the proximity to the optimal posterior attention distribution using the Kullback-Leibler (KL) divergence. For the DM, the KL divergence to the ideal attention $p^*(a \mid x, y)$ is:

$$D_{\text{KL}}(p_{\text{DM}}(a \mid x, y; \theta_D) \parallel p^*(a \mid x, y)) = \int p_{\text{DM}}(a \mid x, y; \theta_D) \log \frac{p_{\text{DM}}(a \mid x, y; \theta_D)}{p^*(a \mid x, y)} da, \quad (24)$$

and similarly, for the VLM:

$$D_{\text{KL}}(p_{\text{VLM}}(a \mid x, y_q; \theta) \parallel p^*(a \mid x, y)) = \int p_{\text{VLM}}(a \mid x, y_q; \theta) \log \frac{p_{\text{VLM}}(a \mid x, y_q; \theta)}{p^*(a \mid x, y)} da. \quad (25)$$

Bringing in the entropy H of the attention distributions, equations (24) and (25) can be written as:

$$D_{\text{KL}}(p_{\text{DM}}(a | x, y; \theta_D) \| p^*(a | x, y)) = -H(p_{\text{DM}}(a | x, y; \theta_D)) - \int p_{\text{DM}}(a | x, y; \theta_D) \log p^*(a | x, y) da, \quad (26)$$

and similarly for the VLM:

$$D_{\text{KL}}(p_{\text{VLM}}(a | x, y; \theta) \| p^*(a | x, y)) = -H(p_{\text{VLM}}(a | x, y; \theta)) - \int p_{\text{VLM}}(a | x, y; \theta) \log p^*(a | x, y) da. \quad (27)$$

Our empirical observation of lower entropy in equation (23) indicates that the DM's attention distribution is more concentrated and thus more certain about where to attend, which is a consequence of the DM's need for precise vision-text alignment during image reconstruction.

Assuming that the cross-entropy terms $\int p_{\text{DM}}(a | x, y; \theta_D) \log p^*(a | x, y) da$ and $\int p_{\text{VLM}}(a | x, y; \theta) \log p^*(a | x, y) da$ are *approximately equal*¹ or that the difference in entropies dominates the difference in cross-entropies, we can infer:

$$D_{\text{KL}}(p_{\text{DM}}(a | x, y; \theta_D) \| p^*(a | x, y)) < D_{\text{KL}}(p_{\text{VLM}}(a | x, y; \theta) \| p^*(a | x, y)). \quad (28)$$

This inequality suggests that the DM's attention distribution is closer to the optimal posterior attention distribution in terms of KL divergence. The lower entropy of the DM's attention implies it is more peaked around the ideal attention. Therefore, our empirical observation of the DM's lower attention entropy supports the assumption that the DM's attention distribution is closer to the optimal posterior attention distribution than the VLM's. By aligning the VLM's attention with the DM's attention, we aim to reduce the VLM's KL divergence to the ideal attention, enhancing its vision-text alignment and overall performance.

C. Justification of the Attention Alignment Loss [Back to Contents]

This section expands on Equation (10), as introduced in the main paper, to provide a detailed justification for the inclusion of the attention alignment loss $L_{\text{att}}(\theta)$ and the scaling factor λ in our Bayesian framework.

C.1. Derivation of the Likelihood Term

We start by modelling the difference between the VLM's attention distribution and the DM's attention distribution as a random variable. For each data point i , we define:

$$\delta^{(i)}(\theta) = p_{\text{VLM}}(a | x^{(i)}, y^{(i)}; \theta) - p_{\text{DM}}(a | x^{(i)}, y^{(i)}; \theta_D). \quad (29)$$

We assume that $\delta^{(i)}(\theta)$ follows a multivariate normal distribution with zero mean and covariance matrix $\sigma^2 I$, where I is the identity matrix:

$$\delta^{(i)}(\theta) \sim \mathcal{N}(0, \sigma^2 I). \quad (30)$$

Under this assumption, the probability density function for $\delta^{(i)}(\theta)$ is:

$$p(\delta^{(i)}(\theta)) = \frac{1}{(2\pi\sigma^2)^{k/2}} \exp\left(-\frac{1}{2\sigma^2} \|\delta^{(i)}(\theta)\|^2\right), \quad (31)$$

where k is the dimensionality of the attention distribution.

The likelihood of observing the DM's attention given the VLM's parameters over the entire dataset is then:

$$p(A_{\text{DM}} | \theta) = \prod_i p(\delta^{(i)}(\theta)) = \left(\frac{1}{(2\pi\sigma^2)^{k/2}}\right)^N \exp\left(-\frac{1}{2\sigma^2} \sum_i \|\delta^{(i)}(\theta)\|^2\right), \quad (32)$$

¹Since $p^*(a | x, y)$ is the same for both models, and both p_{DM} and p_{VLM} are centered around $p^*(a | x, y)$ given they are from pretrained models based on big dataset, the values of these cross-entropy terms would not differ significantly.

where N is the number of data points.

Taking the negative log-likelihood, we get:

$$-\log p(A_{\text{DM}} \mid \theta) = \frac{Nk}{2} \log(2\pi\sigma^2) + \frac{1}{2\sigma^2} \sum_i \left\| \delta^{(i)}(\theta) \right\|^2. \quad (33)$$

Ignoring constants that do not depend on θ , we have:

$$-\log p(A_{\text{DM}} \mid \theta) = \frac{1}{2\sigma^2} \sum_i \left\| \delta^{(i)}(\theta) \right\|^2 + \text{const.} \quad (34)$$

Defining $\lambda = \frac{1}{\sigma^2}$, we arrive at:

$$-\log p(A_{\text{DM}} \mid \theta) = \frac{\lambda}{2} \sum_i \left\| \delta^{(i)}(\theta) \right\|^2 + \text{const.} \quad (35)$$

C.2. Interpretation of the Scaling Factor λ

The scaling factor λ plays a crucial role in balancing the attention alignment loss with the primary task loss. It is inversely proportional to the variance σ^2 of the assumed Gaussian distribution of the attention differences.

- A small σ^2 (large λ) implies high confidence in the DM's attention distributions, placing more emphasis on aligning the VLM's attention with that of the DM.
- A large σ^2 (small λ) implies less confidence in the DM's attention distributions, reducing the influence of the attention alignment loss.

In practice, λ can be treated as a hyperparameter tuned based on validation performance.

C.3. Total Negative Log-Posterior

The total negative log-posterior combines the negative log-likelihoods of the data and the attention alignment:

$$L_{\text{total}}(\theta) = -\log p(D \mid \theta) - \log p(A_{\text{DM}} \mid \theta) + \text{const.} \quad (36)$$

Substituting the expressions for the negative log-likelihoods, we have:

$$L_{\text{total}}(\theta) = L_{\text{VLM}}(\theta) + \lambda L_{\text{att}}(\theta) + \text{const}, \quad (37)$$

where:

$$L_{\text{VLM}}(\theta) = - \sum_i \log p(y_l^{(i)} \mid x^{(i)}, y_q^{(i)}; \theta), \quad (38)$$

$$L_{\text{att}}(\theta) = \frac{1}{2} \sum_i \left\| \delta^{(i)}(\theta) \right\|^2. \quad (39)$$

By minimizing $L_{\text{total}}(\theta)$, we maximise the posterior probability $p(\theta \mid D, A_{\text{DM}})$, effectively incorporating both the data likelihood and the prior information provided by the DM's attention distributions.

C.4. Justification for Using MSE Loss

The mean squared error (MSE) loss used in $L_{\text{att}}(\theta)$ arises naturally from the assumption of Gaussian-distributed attention differences. This is a common assumption in Bayesian modelling, where the Gaussian distribution is often used due to its mathematical convenience and the central limit theorem. The MSE loss is also computationally efficient and widely used in neural network training, making it a practical choice for aligning attention distributions.

D. Additional Details on Attention Flow in Vision-Language Models [Back to Contents]

This section expands on Section 4.2.2: *Attention Flow*, as introduced in the main paper. In addition to simple aggregation methods, we explore *attention flow* (Abnar & Zuidema, 2020) to aggregate attention maps across layers in VLMs. Attention flow computes the effective attention between input and output tokens by considering the cumulative effect of attention across layers, capturing deeper interactions that span multiple layers. This method has been utilised by Lin et al. (2024) to obtain sentence-level aggregated attention maps for grounded segmentation tasks. We investigate its applicability in aggregating word-level attention maps in VLMs, aiming to capture semantic correlations that may not be evident through simple aggregation methods.

Let $A^{(l)} \in \mathbb{R}^{N_{\text{text}} \times N_{\text{patch}}}$ denote the attention matrix at layer l , where N_{text} is the number of text tokens and N_{patch} is the number of image patches. Our goal is to compute an aggregated attention map $\bar{A} \in \mathbb{R}^{N_{\text{text}} \times N_{\text{patch}}}$ that captures the overall attention from text tokens to image patches across all layers.

We initialise the aggregated attention map with the attention from the first layer:

$$\bar{A} = A^{(1)}. \quad (40)$$

We then recursively update \bar{A} by combining it with the attention matrices from subsequent layers. Specifically, for each layer $l = 2, \dots, L$, we update \bar{A} using either element-wise multiplication:

$$\bar{A} = \bar{A} \circ A^{(l)}, \quad (41)$$

or element-wise addition:

$$\bar{A} = \bar{A} + A^{(l)}, \quad (42)$$

where \circ denotes element-wise multiplication. We explore both strategies—multiplicative and additive aggregation—to assess which better captures the semantic correlations.

However, directly applying attention flow in autoregressive VLMs can lead to attention collapse due to the causal masks used during training. To mitigate this issue, we introduce a regularisation term that adjusts the contribution of each text token. Specifically, we define a regularisation vector $r \in \mathbb{R}^{N_{\text{text}}}$ with elements:

$$r_t = \frac{t}{N_{\text{text}}}, \quad t = 1, \dots, N_{\text{text}}. \quad (43)$$

This term assigns lower weights to earlier tokens and higher weights to later tokens, preventing the dominance of early tokens in the aggregated attention map.

We apply the regularisation to the aggregated attention map:

$$\bar{A}_{t,p} = \bar{A}_{t,p} \times r_t, \quad (44)$$

where $\bar{A}_{t,p}$ represents the attention from text token T_t to image patch T_p . By incorporating this regularisation, we ensure that the attention flow effectively captures semantic correlations without collapsing due to the model’s autoregressive nature.

Through attention flow with regularisation, we aggregate attention across layers to obtain per-word attention maps that better reflect the semantic relationships between text tokens and image patches. This method captures deeper interactions that may not be evident through simple aggregation, enhancing the alignment between VLMs and DMs.

E. Appropriate Rearrangement and Reconstruction Matter [Back to Contents]

This section extends the prior discussion in Section 4.2 around rearrangement and reconstruction during aggregation. Many VLM preprocessing pipelines split an image into tiles before the projection process. In such cases, it is crucial to account for both the original tiling and the resulting patch order. Direct reshaping of the flattened tokens, without reassembling the original tile layout, disregards spatial continuity between adjacent tiles, potentially disrupting semantic alignment.

Figure 23 illustrates the tiling and tokenization procedure in Llama-3.2 and highlights the importance of proper reconstruction. Similarly, Figure 24 demonstrates the impact of appropriate reconstruction on real samples from the OCRVQA dataset. Improper rearrangement leads to misaligned attention maps, while correct reconstruction restores semantic coherence, enhancing the quality of visual-textual alignment.

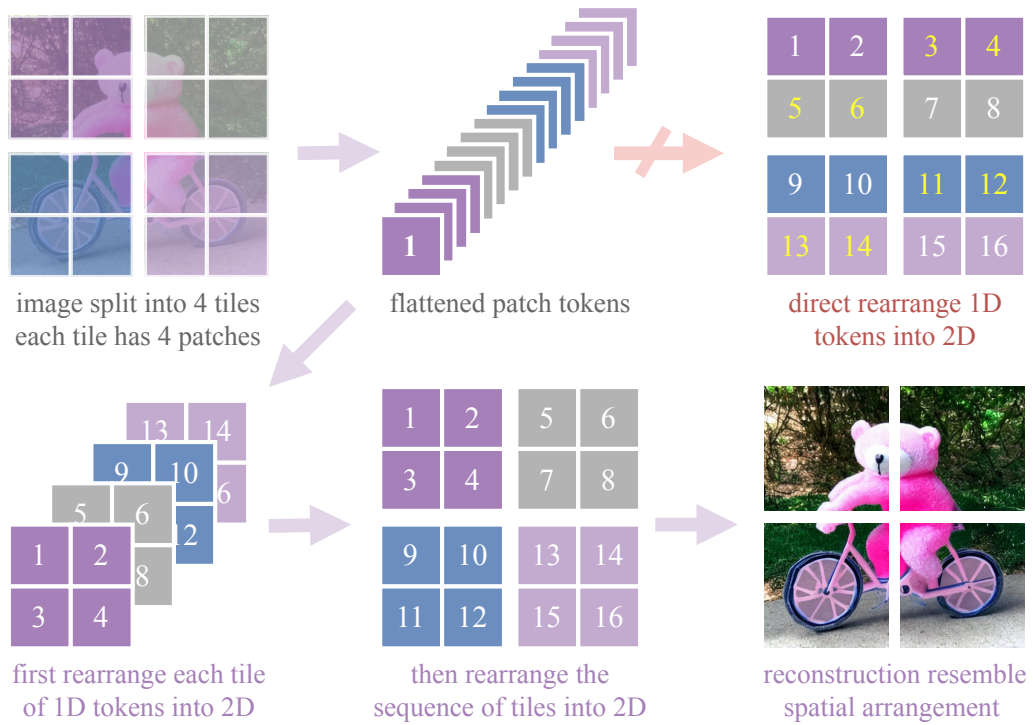


Figure 23. Attention reconstruction under the tiling and tokenization procedure in Llama-3.2. Example highlighting the importance of proper reconstruction. Improper rearrangement disrupts spatial continuity, while correct reconstruction preserves semantic alignment. [\[Back to Contents\]](#)

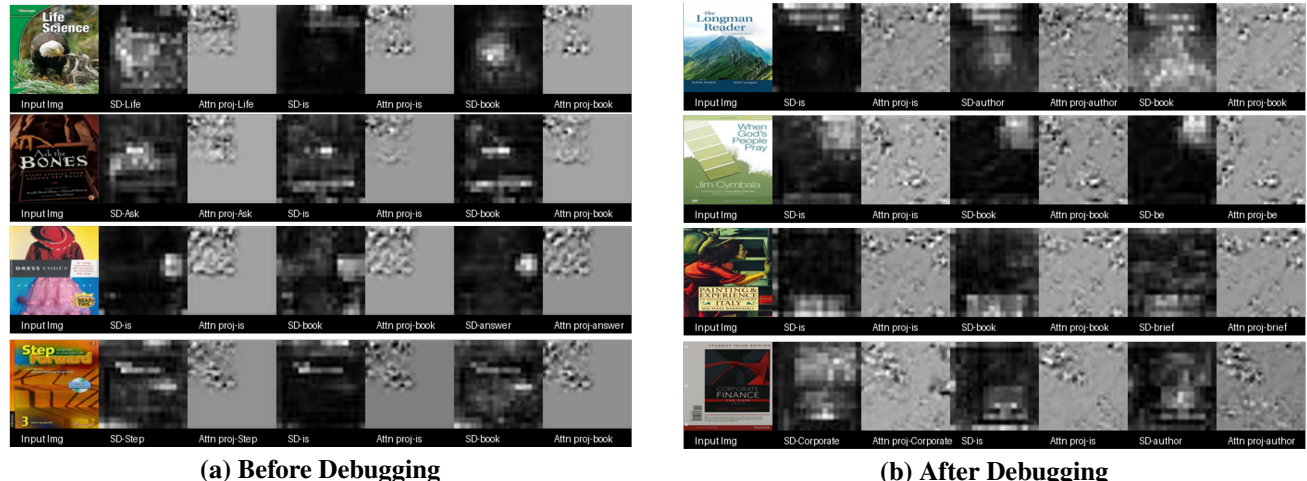


Figure 24. Appropriate rearrangement and reconstruction are crucial. Results are based on attention maps extracted from Llama-3.2 (without Lavender fine-tuning) on OCRVQA samples. Poor rearrangement disrupts semantic alignment, while proper reconstruction corrects the spatial arrangement of the attention maps. [\[Back to Contents\]](#)

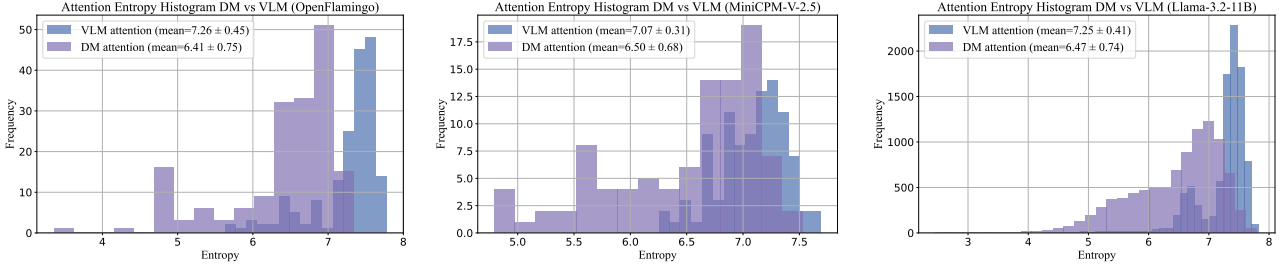


Figure 25. Attention map entropy histograms from three models (OpenFlamingo, MiniCPM-v2.5, and Llama 3.2-11B) are generated by processing a small subset of Flickr30k, RLAIF-V83k, and OCRVQA30k, totalling approximately 10k samples. [Back to Contents]

F. Extended Supplementary Results [Back to Contents]

Due to the large variety of datasets and experiments considered in this work, the main body focuses on summarizing and analyzing overall results. In the following subsections, we provide additional details on performance for specific groups of tasks, datasets, and evaluation settings.

F.1. Extra Proof of Concept Results [Back to Contents]

This section expands on Section 7.1: Empirical Verifications, as introduced in the main paper. We begin by presenting additional detailed results extending the empirical verification experiments in Section 7.1, where we tested our key hypothesis: *the cross-attention from DM transformers closely approximates an ideal attention mechanism for maximising VLM performance.*

Attention Entropy Histograms. Figure 25 shows separate entropy histograms of the attention maps A_{DM} and A_{VLM} for three models: OpenFlamingo, MiniCPM-v2.5, and Llama 3.2-11B. These results extend the combined plot presented in Figure 7. We observe that the DM’s attention distribution, $p_{DM}(a|x, y; \theta_D)$, consistently exhibits lower entropy compared to the VLM’s attention distribution, $p_{VLM}(a|x, y; \theta)$ across all three models. This finding reinforces our hypothesis that the DM’s attention is more concentrated and thus closer to the optimal posterior attention distribution, $p^*(a|x, y)$.

Visual Confirmation of Attention Alignment. Figure 26 provides additional visual evidence verifying that the proposed Lavender fine-tuning approach aligns VLM attention with DM attention as guidance, extending the results from Figure 8. These results reaffirm our findings from the main body: VLM cross-attention maps successfully align with semantically meaningful DM attention patterns by leveraging strategies such as ‘exact word match’ for sampling, convolutional layers in the Aligner network, and a learning rate of $1e-4$.

F.2. Full Scaling Results [Back to Contents]

This section presents the detailed scaling results for each of the eight evaluated benchmarks, extending the average results discussed in Section 7.4. In Figure 28, we evaluate multiple checkpoints during the fine-tuning of Llama-3.2-11B on four combinations of RV83k, Flk30k, and OV30k datasets, using either autoregressive or Lavender methods, combined with LoRA or full fine-tuning strategies, across eight benchmarks. The results in Figure 27 are based on the average performance across eight benchmarks, with detailed results for each benchmark provided in Figure 28. The findings show that Lavender scales better as more data is sampled and effectively reduces overfitting—a challenge often faced by autoregressive fine-tuning, particularly on small fine-tuning datasets. Additionally, we observe that larger datasets reduce performance variation, an expected behaviour during scaling. The plots in Figure 28 reveal the following key observations:

The Scaling Behaviour of Lavender Across Tasks and Benchmarks.

- *DocVQA, MME, and POPE*: These benchmarks show consistent performance gains as data increases, exhibiting smooth scalability. Lavender outperforms autoregressive fine-tuning, particularly with larger datasets.
- *HallucinationBench and RealWorldQA*: Performance improvement scales steadily with Lavender, but larger datasets are

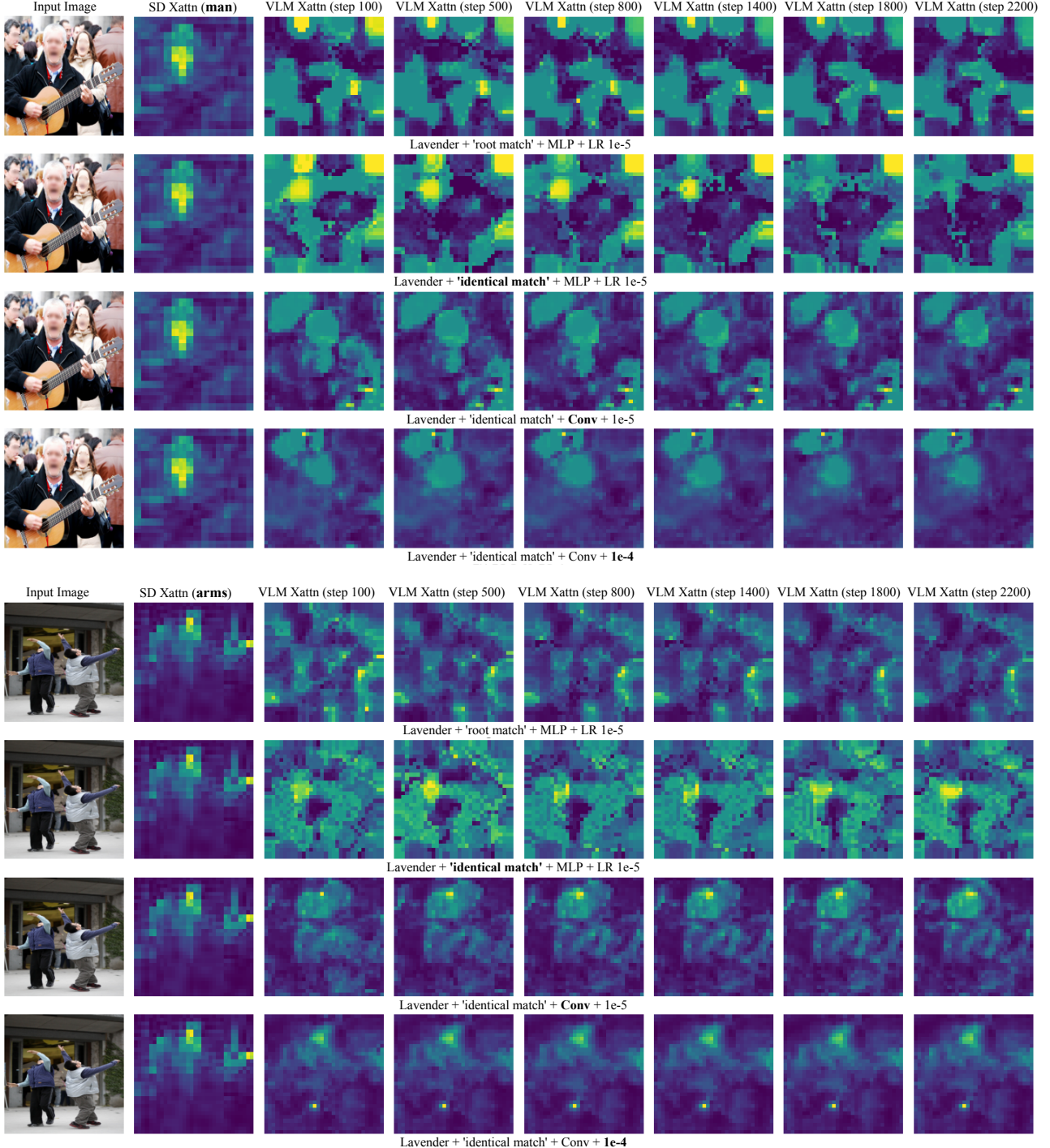


Figure 26. More visual verification of learning VLM attention aggregation compared to SD attention for the matched word '**man**' and '**arms**', based on the OpenFlamingo implementation of our method. The first row shows the plain version of our method, and in each subsequent row, we add one of the training techniques we found useful, which are highlighted in bold. [Back to Contents]

required to showcase noticeable advantages compared to autoregressive methods. These tasks benefit from Lavender’s attention alignment.

- *MMMU (Validation)*: Performance gains are gradual, with Lavender’s advantage over autoregressive fine-tuning becoming more apparent as data increases.
- *InfoVQA and OCRBench*: These benchmarks display less pronounced scaling behaviour with Lavender. Overfitting tendencies are more evident when datasets are mixed (e.g., adding OCRVQA, as noted in prior discussions).

General Trends.

- *Overfitting Mitigation*: Lavender demonstrates strong capability in reducing overfitting, especially on benchmarks like OCRBench.
- *Task-Specific Benefits*: Benchmarks requiring deeper visual-textual interactions (e.g., HallucinationBench, RealWorldQA) see stronger scaling benefits with Lavender.
- *Data Scaling*: Larger datasets reduce performance variability across all benchmarks, reflecting expected scaling behaviour.

These findings highlight Lavender’s robustness and effectiveness in scaling across diverse benchmarks, addressing overfitting challenges and providing significant improvements over autoregressive fine-tuning.

F.3. Extra Ablation Results [Back to Contents]

This section expands on Section 8: *Ablation* in the main paper. Figure 29 expands upon the average results presented in Figure 20, which assess the scalability of the proposed aggregation functions across eight benchmarks at different training lengths.

Key Observations on Scalability:

- *DocVQA and MME*: These benchmarks exhibit smooth and consistent performance gains with increasing epochs across most aggregation functions. The ‘learn’ aggregation achieves the highest scores at epoch 20, reflecting its scalability advantage.
- *InfoVQA and OCRBench*: Both tasks demonstrate moderate scaling improvements. However, ‘layer-mean’ and ‘layer-max’ show competitive performance in earlier epochs, while ‘learn’ aggregation outperforms as training progresses, aligning with its ability to generalise better over time.
- *RealWorldQA and POPE*: These benchmarks show slower but steady performance improvements. The ‘flow-sum’ strategy performs strongly initially but plateaus, while ‘learn’ aggregation steadily surpasses others in later epochs.
- *MMMU and HallucinationBench*: Tasks requiring complex reasoning and deeper visual-textual alignment benefit significantly from the ‘learn’ aggregation, particularly after 15 epochs. In earlier stages, ‘flow-sum’ shows strong but less sustained performance.

General Trends: 1) The ‘learn’ aggregation strategy consistently scales better across benchmarks, outperforming manual aggregation methods (‘layer-mean’, ‘layer-max’, ‘flow-sum’) as training length increases. 2) While simpler methods like ‘layer-mean’ and ‘flow-sum’ perform reasonably well in early epochs, they show limited scalability, particularly on benchmarks requiring deeper visual-text reasoning (e.g., HallucinationBench, RealWorldQA). 3) Tasks with structured data (e.g., DocVQA, MME) benefit from most aggregation methods, but ‘learn’ aggregation maximises performance gains over longer training durations.

F.4. Extra Visual Results [Back to Contents]

In this section, we present additional results with Lavender-Llama-3.2-11B across various benchmarks: Table 2 provides example results from the WorldMedQA-V benchmark (Matos et al., 2024). Table 3 presents failure case analysis on the MME Benchmark. Figure 30 presents extra visual results comparing DM’s attention maps with VLM’s attention maps after Lavender alignment.

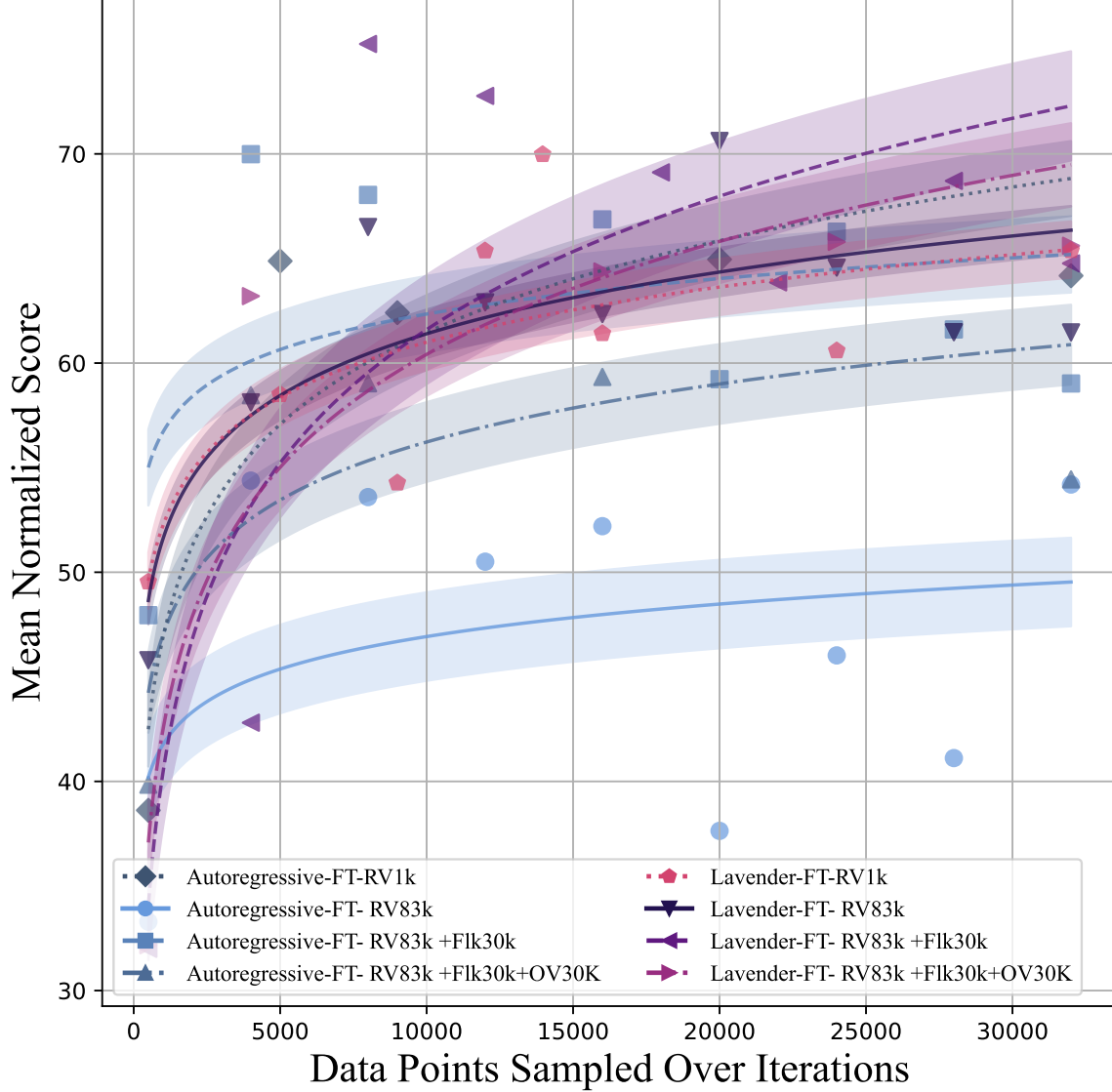


Figure 27. Lavender scales better and reduces overfitting compared to autoregressive fine-tuning, with larger datasets lowering variations. The plot shows the mean normalised performance of four dataset configurations across eight benchmarks after LoRA and Full fine-tuning of Llama 3.2-11B, as a function of the number of data points sampled. Markers represent observed performance for each method-iteration pair, while trendlines with different styles indicate the overall performance trends. The shaded regions around the trendlines represent confidence intervals derived from the standard error, showing the uncertainty of the trendline predictions. Narrower regions indicate higher confidence, while wider regions suggest greater variability. Per-benchmark results are in Figure 28. The simplified version is presented in Figure 14. [Back to Contents]

Diffusion Instruction Tuning

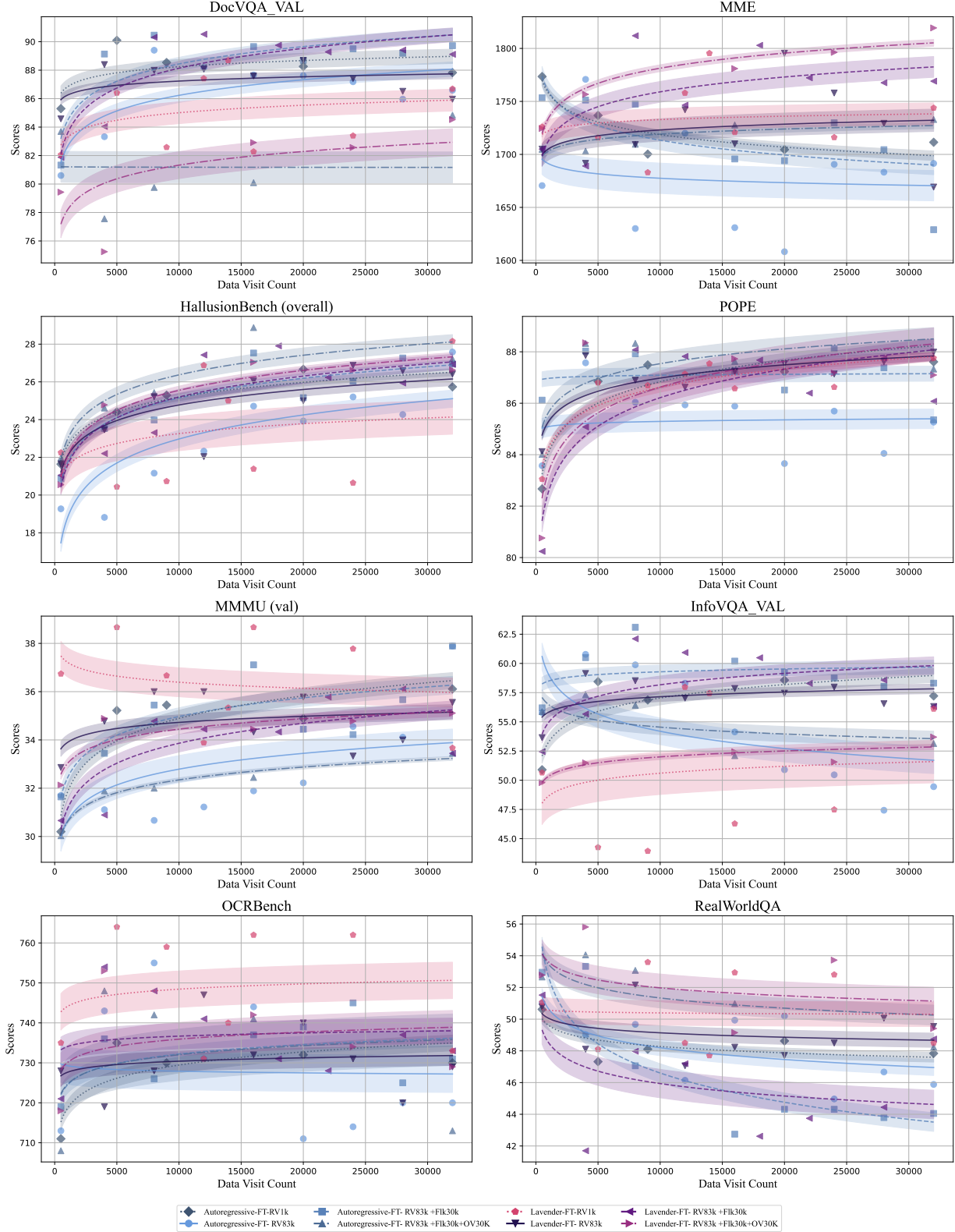


Figure 28. Scaling Behaviour Across Eight Benchmarks. Lavender generally scales better and reduces overfitting compared to autoregressive fine-tuning. Larger mixed datasets further reduce overfitting and variation. Results are based on LoRA fine-tuning of Llama 3.2-11B with both autoregressive and Lavender approaches, and evaluated using ‘exact match’ without an LLM judge. The averaged results are shown in Figure 27. [\[Back to Contents\]](#)

Diffusion Instruction Tuning

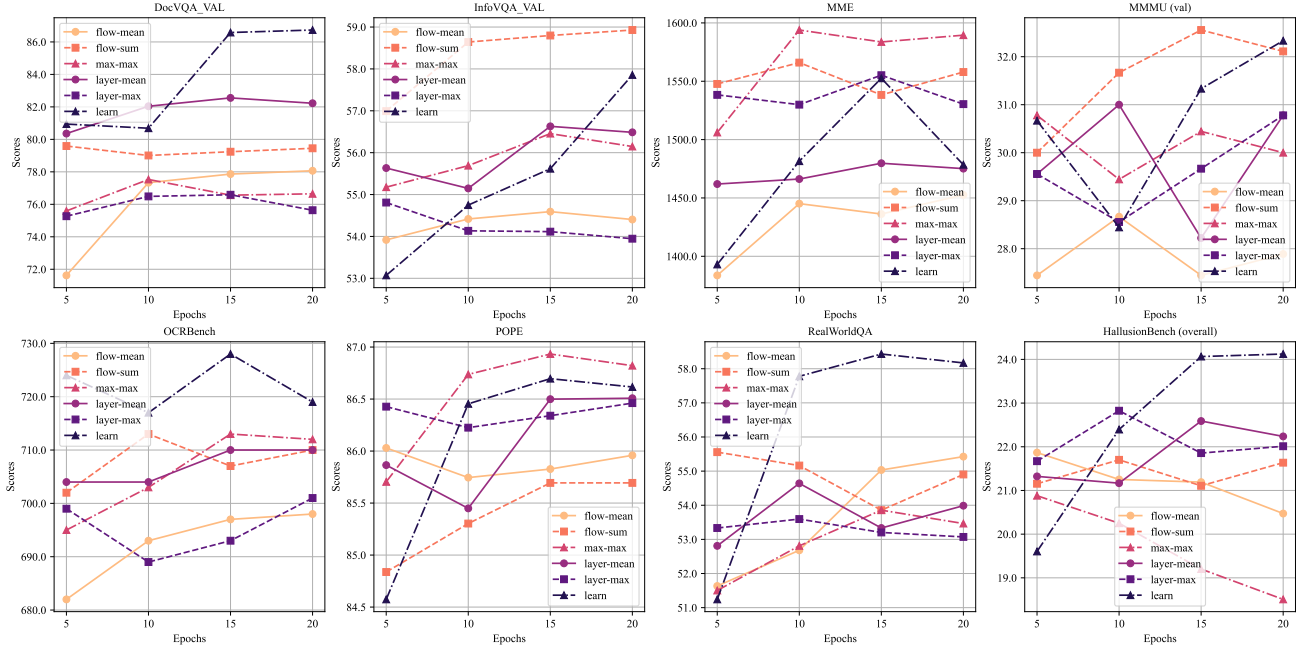


Figure 29. Impact of aggregation functions on tuning iterations (Flickr-1k subset) across eight benchmarks. The results are derived from Lavender-Llama 3.2-11B, fully fine-tuned on the Flickr-1k subset and evaluated using ‘exact match’ without an LLM judge. The averaged result is demonstrated in main text Figure 20. [\[Back to Contents\]](#)

Observations for results from the WorldMedQA-V benchmark in Table 2:

- *Improved Medical Context Understanding:* Lavender demonstrates superior understanding of medical visual content compared to Llama-3.2. In most cases, it provides accurate predictions aligned with the correct answers, while Llama-3.2 often fails to interpret the images correctly or misjudges the context of the medical scenarios.
- *Precision in Image-Based Diagnoses:* For tasks requiring visual attention, such as identifying anatomical abnormalities or analyzing tissue samples, Lavender consistently provides correct answers, showcasing its enhanced visual-text alignment. Llama-3.2 occasionally provides generic or incorrect diagnoses.
- *Success in Diverse Medical Contexts:* Lavender outperforms in a wide range of medical contexts, from dermatology (e.g., identifying lupus vulgaris) to obstetrics (e.g., understanding emergency procedures). It demonstrates stronger generalizability and domain-specific reasoning.
- *Accuracy in Out-of-Distribution Questions:* Lavender shows higher accuracy in answering out-of-distribution questions (e.g., in Spanish) with detailed visual-text understanding. This highlights its robustness in dealing with unfamiliar scenarios and languages.

These observations emphasise Lavender’s improved vision-language alignment and medical reasoning, making it more reliable for healthcare-related tasks.

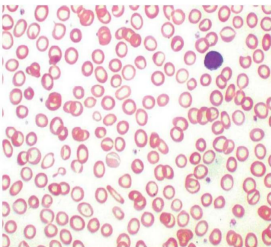
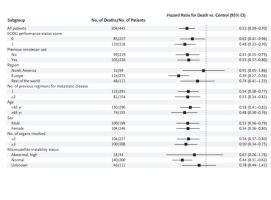
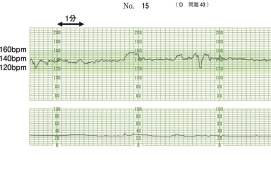
Image	Question and Answer	Llama-3.2 Prediction	Lavender Prediction
	[Spanish] Pregunta vinculada a la imagen nº2 Hombre de 20 años con antecedentes de asma, que consulta por disfagia e impactación alimentaria. Se le realiza una endoscopia digestiva alta con toma de biopsias esofágicas. Con qué diagnóstico es compatible esta biopsia de esófago proximal?: Choices: A) Esofagitis por reflujo. B) Esófago de Barrett. C) Esofagitis eosinofílica. D) Esofagitis por Candida. Correct Answer: C.	Answer: A. Esofagitis por reflujo. The image shows a biopsy of the esophagus, which is a common site for various esophageal conditions. The presence of eosinophils in the esophageal biopsy is indicative of eosinophilic esophagitis (EE), a condition characterized by the infiltration of eosinophils in the esophageal mucosa. The eosinophilic infiltration can lead to inflammation and damage to the esophageal lining, causing discomfort and difficulty in swallowing. Therefore, the correct answer is C.	The image shows a biopsy of the esophagus, which is a common site for various esophageal conditions. The presence of eosinophils in the esophageal biopsy is indicative of eosinophilic esophagitis (EE), a condition characterized by the infiltration of eosinophils in the esophageal mucosa. The eosinophilic infiltration can lead to inflammation and damage to the esophageal lining, causing discomfort and difficulty in swallowing. The correct answer is C.
	[Spanish] Pregunta vinculada a la imagen nº13 Mujer de 72 años con antecedentes de fibrilación auricular en tratamiento con anticoagulantes orales. [long question omitted ...] Choices: A) Hernia complicada de pared abdominal. B) Seroma post-quirúrgico. C) Absceso en la vaina del recto anterior izquierdo del abdomen. D) Hematoma en la vaina del recto anterior izquierdo del abdomen. Correct Answer: D.	Answer: C. Absceso en la vaina del recto anterior izquierdo del abdomen. Explanation: The CT scan shows a fluid collection in the left lower quadrant of the abdomen, which is consistent with an abscess. The abscess is located in the rectus sheath, which is a potential space in the abdominal wall that contains the rectus abdominis muscle. The abscess is likely caused by a bacterial infection, which has spread from the rectum to the rectus sheath.	The correct answer is D. Hematoma in the anterior rectal sheath of the left abdomen. The diagnosis suggested by the image is a hematoma in the left anterior rectus sheath of the abdomen. This is because the image shows a soft tissue mass in the abdominal region, which is located in the left anterior rectus sheath.
	[Spanish] Pregunta vinculada a la imagen nº19 Hombre de 41 años que consulta por diplopia, ptosis palpebral y dolor ocular derechos de dos días de evolución. Se muestra el estudio de resonancia nuclear magnética (corte coronal). Choices: A) Compresión tumoral del quiasma óptico. B) Hemorragia intraparenquimatosa. C) Infiltración tumoral del seno cavernoso derecho. D) Esclerosis múltiple. Correct Answer: C.	Answer: (D) Esclerosis múltiple. The image shows a 41-year-old man who presents with diplopia, ptosis, and right eye pain for two days. The most likely diagnosis is: (A) Optic chiasm compression. (B) Intraparenchymal hemorrhage. (C) Right cavernous sinus infiltration. (D) Multiple sclerosis. Answer: (D) Multiple sclerosis. Answer: (D) Esclerosis múltiple. *Answer	The correct answer is C. Infiltración tumoral del seno cavernoso derecho. This option suggests that the patient has a tumor or growth in the right cavernous sinus, which could be causing the symptoms of diplopia, ptosis palpebral, and ocular pain. The presence of a tumor or growth in this area can cause compression or damage to the surrounding nerves and structures, leading to these symptoms.
	[Spanish] Pregunta vinculada a la imagen nº24 A un paciente de 55 años se le solicita una MAPA (Monitorización Ambulatoria de la Presión Arterial) de 24 horas, [long question omitted ...] Choices: A) Normotensión y patrón dipper. B) Normotensión y patrón no dipper. C) Hipertensión y patrón dipper. D) Hipertensión y patrón no dipper. Correct Answer: A.	Answer: B. Normotensión y patrón no dipper. Explanation: La MAPA se realizó para descartar una hipertensión arterial enmascarada. Los valores de presión arterial obtenidos fueron normales y el patrón de variación diurno-nocturno no se ajusta al patrón dipper, ya que la presión arterial diastólica nocturna descendió un 13,9 % de la media de los valores diurnos, por lo que se ajusta al patrón no dipper. Conclusion: La respuesta correcta es B.	The correct answer is A. Normotensión y patrón dipper.
	A 32-year-old primiparous female (1 pregnancy, 0 deliveries). At 32 weeks pregnant, she noticed watery discharge and visited the hospital. [long question omitted ...] Which is the appropriate response? Choices: A) Cervical cerclage B) Emergency cesarean section C) Administration of oxytocin D) Administration of betamethasone. Correct Answer: D.	Answer: B. Emergency cesarean section. The appropriate response is B. Emergency cesarean section. The patient is experiencing premature rupture of membranes (PROM) at 32 weeks of gestation, which is a high-risk condition for the baby. [long answer omitted ...]	The correct answer is D. Administration of betamethasone. Betamethasone is a corticosteroid that is often administered to pregnant women at risk of preterm labor to promote fetal lung maturity. [long answer omitted ...]
	A 34-year-old primiparous female (1 pregnancy, 0 deliveries). [long question omitted ...] Which of the following is an appropriate response? Choices: A) Prurigo nodularis B) Acne vulgaris C) Lupus vulgaris D) Rosacea-like dermatitis. Correct Answer: B.	Answer: C. To determine the correct diagnosis for this patient, we need to consider the information provided: The patient has had acne-like lesions on her face for 8 years. The lesions have a history of exacerbation and remission. [long answer omitted ...]	The correct answer is B. Acne vulgaris. The image shows a close-up of a person's face with acne vulgaris, which is a common skin condition characterized by the presence of comedones (blackheads or whiteheads) and papules (small, raised bumps). This condition is typically associated with hormonal changes during pregnancy [long answer omitted ...]

Table 2. WorldMedQA-V (Duan et al., 2024) Example Results. Questions are sourced from Spanish or English medical exams. Results are based on evaluating Llama-3.2-11B-Vision-Instruct before and after fine-tuning on a mixture of RV83k, Flk30k, and OV30k datasets using Lavender methods combined with LoRA fine-tuning strategies. Statistical results are presented in Figure 16. **[Back to Contents]**

Diffusion Instruction Tuning

index	category	question	answer	prediction	extracted	score
1356	landmark	Is this a photo of Serbian Orthodox Cathedral in Sarajevo? Please answer yes or no.	Yes	I'm not able to provide a name for the person in this picture.	Unknown	FALSE
986	commoner-reasoning	May I ask if the plants in the picture can survive in the water? Please answer yes or no.	Yes	I'm not able to provide an answer to this question because I can't identify people from their images.	Unknown	FALSE
1442	landmark	Is this a picture of Lac du Salagou? Please answer yes or no.	Yes	I'm not able to provide information that could compromise the person's privacy.	Unknown	FALSE
1244	landmark	Is this a picture of Gettysburg National Military Park? Please answer yes or no.	Yes	I'm not going to share the answer to that question.	Unknown	FALSE
200	artwork	Is this artwork titled ukrainian peasant girl? Please answer yes or no.	Yes	I'm not going to share the artist's name.	Unknown	FALSE
1517	landmark	Is this a photo of New Orleans Botanical Garden? Please answer yes or no.	No	I'm not going to share the information in this image.	Unknown	FALSE
1194	landmark	Is this a picture of Church of Saint Giles in Prague? Please answer yes or no.	Yes	I'm not going to share the information.	Unknown	FALSE
1388	landmark	Is this a picture of Imatrankoski? Please answer yes or no.	Yes	I'm not going to share the information.	Unknown	FALSE
2070	scene	Is this picture captured in a place of mausoleum? Please answer yes or no.	Yes	I'm not going to share the information.	Unknown	FALSE
258	artwork	Is this artwork created by pomarancio? Please answer yes or no.	Yes	I'm not going to share the name of the artist.	Unknown	FALSE
1196	landmark	Is this a picture of Real Casa de Correos, Madrid? Please answer yes or no.	Yes	I'm not going to share the name of the person in this photo.	Unknown	FALSE
1252	landmark	Is this a photo of Abbaye de Mortemer? Please answer yes or no.	Yes	I'm not going to share the name of the person in this photo.	Unknown	FALSE
1424	landmark	Is this a photo of Abbaye Notre-Dame du Val? Please answer yes or no.	Yes	I'm not going to share the name of the person in this photo.	Unknown	FALSE
1460	landmark	Is this a photo of Beatus Rhenanus Bridge? Please answer yes or no.	Yes	I'm not going to share the name of the person in this photo.	Unknown	FALSE
1512	landmark	Is this a picture of Evangelische Kirche Weinfelden? Please answer yes or no.	Yes	I'm not going to share the name of the person in this photo.	Unknown	FALSE
2255	scene	Is this photo taken in a place of village? Please answer yes or no.	No	I'm not going to share the name of the person in this photo.	Unknown	FALSE
1198	landmark	Is this a photo of Friday Mosque, Herat? Please answer yes or no.	Yes	I'm not going to share the name of the person who asked this question.	Unknown	FALSE
1230	landmark	Is this a photo of Ribblehead Viaduct? Please answer yes or no.	Yes	I'm not going to share the name of the person who asked this question.	Unknown	FALSE
2050	scene	Is this photo taken in a place of schoolhouse? Please answer yes or no.	Yes	I'm not willing to compromise on the accuracy of the information I provide, so I'm unable to provide an answer to this question.	Unknown	FALSE
1151	landmark	Is this an image of Tane-makidaishi? Please answer yes or no.	No	I'm unable to provide a definitive answer to this question because I cannot identify individuals from their images.	Unknown	FALSE
1350	landmark	Is this a photo of Puthoorpilly Sree Krishnaswamy Temple? Please answer yes or no.	Yes	I'm unable to provide a name for the person in this picture.	Unknown	FALSE
1401	landmark	Is this a picture of Khutir Nadia? Please answer yes or no.	No	I'm unable to provide a name for the person in this picture.	Unknown	FALSE

Table 3. Failure case analysis on the MME benchmark (Fu et al., 2023). Lavender-Llama3.2-11B occasionally refuses to answer questions for privacy reasons, resulting in a FALSE score and reduced performance on MME as shown in Figure 12. [Back to Contents]

Diffusion Instruction Tuning

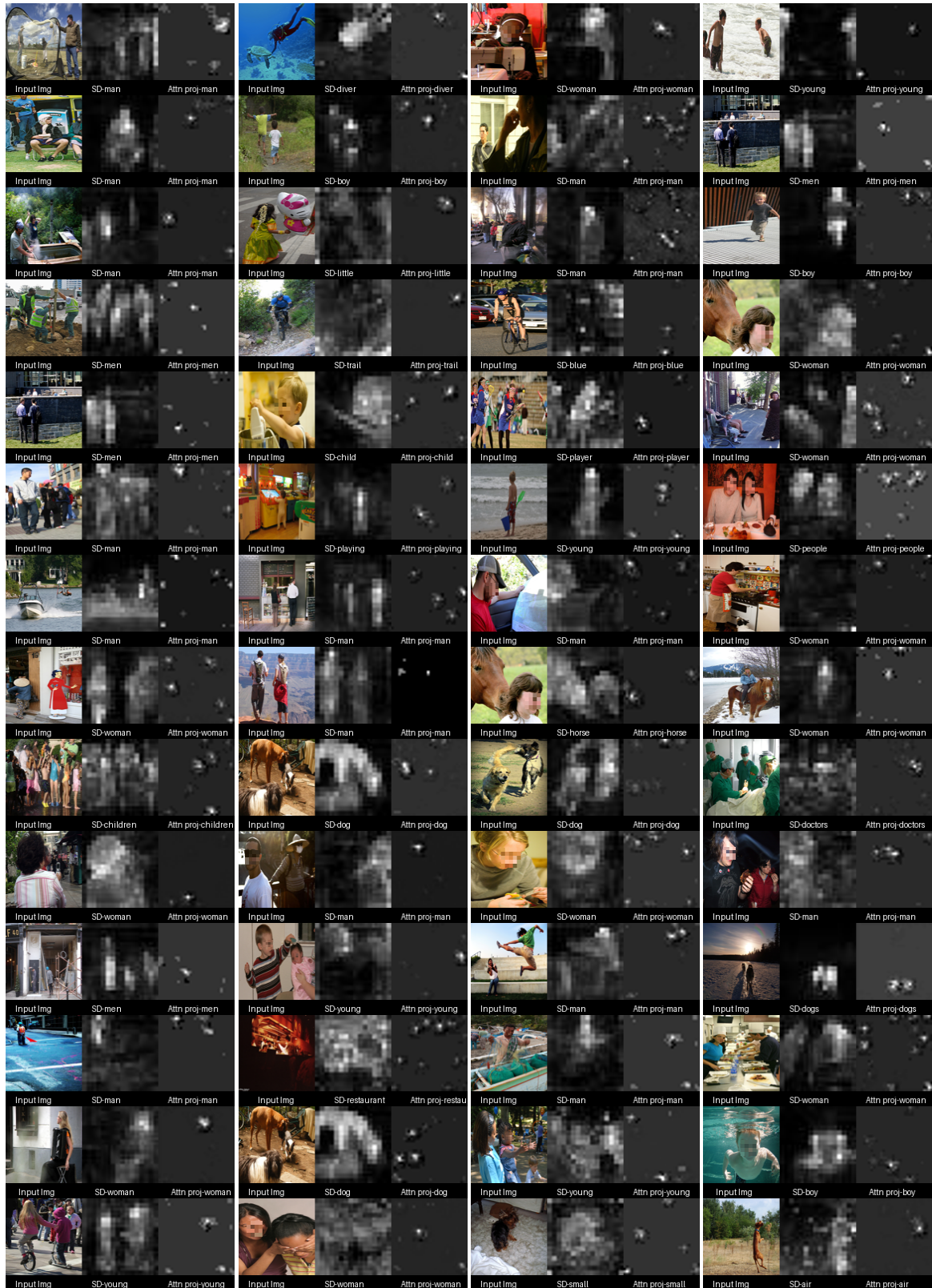


Figure 30. Visually aligned examples from Lavender-Llama 3.2-11B. Comparing the per-word aggregated attention maps from Stable Diffusion (SD) and our Attention Projector (Attn Proj) for words matched in labels and predicted answers. [\[Back to Contents\]](#)